Bistatisk SAR-system med stasjonær mottaker

Georg G Strømsmo og Øyvind Thingsrud

Forsvarets forskningsinstitutt (FFI)

22. oktober 2012

FFI-rapport 2012/01943

124801

P: ISBN 978-82-464-2143-8
E: ISBN 978-82-464-2144-5

Emneord

Syntetisk aperture radar (SAR)

Tilpasset filter

Ulineær dopplerskift kompensering

Bistatisk

Dopplereffekt

Godkjent av

Tor-Odd Høydal	Prosjektleder
Anders Eggen	Avdelingssjef

Sammendrag

Denne rapporten inneholder Georg G. Strømsmos masteravhandling som ble skrevet under hans masterarbeid ved Høgskolen i Narvik (HiN) med ferdigstillelse 1. juli 2012. Arbeidet og avhandlingen *"Bistatic SAR with Stationary Receiver"* ble utført ved Forsvarets forskningsinstitutt under prosjekt 1248 – "Operativ EK-støtte til Forsvaret III" (OPEK III).

Et bistatisk SAR-system kan implementeres ved kun lytting på et eksisterende SAR-system og dens produserte refleksjoner fra terrenget, og deretter kan et SAR-bilde prosesseres frem.

Avhandlingen beskriver både tradisjonell monostatisk og bistatisk SAR-geometri, og deres prosessering og metoder spesielt for forbedring av det bistatiske SAR-bildet.

English summary

This thesis for the Master degree at Høyskolen i Narvik (HiN) was written by Georg G. Strømsmo during his work on *"Bistatic SAR with Stationary Receiver"* at the Norwegian Defence Research Establishment (FFI) with completion date 1st July 2012.

A bistatic SAR-system can be implemented with just listening to an existing SAR-system and its reflections from the ground, and then a SAR-image can be produced.

The thesis describes both the traditional monostatic and the bistatic SAR geometry and their processing, and methods for improvement of the bistatic SAR image.

Innhold

1 Innledning 7

Appendix A Masteravhandling 8

1 Innledning

Denne rapporten inneholder en masteravhandling med tittel *"Bistatic SAR with Stationary Receiver"* som ble skrevet av Georg G. Strømsmo under hans masterstudium ved Høgskolen i Narvik (HiN), avdeling for teknologi. Arbeidet ble utført under veiledning av førsteamanuensis Raymond Kristiansen (HiN), forsker Øyvind Thingsrud (FFI) og forsker Stein Kristoffersen (FFI) ved Forsvarets forskningsinstitutt under prosjekt 1248 – Operativ EK-støtte til Forsvaret III (OPEK III).

Avhandlingen omhandler en såkalt haikende bistatisk syntetisk aperture radar (SAR) hvor SAR-bildet blir prosessert av data innsamlet ved kun lytting på et eksisterende fly- eller satellittbasert SAR-system og dens produserte refleksjoner fra terrenget mottatt med en stasjonær mottaker. En haikende SAR er dermed helt passiv med alle de fordeler dette medfører som lav kompleksitet og kostnad, men signalprosesseringen blir dermed mye vanskeligere siden geometrien mellom radarsender og mottaker endres hele tiden. Det finnes heller ingen synkronisering mellom sender og mottaker foruten selve radarpulsene.

Arbeidene beskriver tradisjonell monostatisk SAR-radar og dens prosessering, og hva som blir forskjellig i det bistatiske oppsettet. Et bistatisk SAR-bilde blir deretter produsert ved hjelp av et dataopptak fra belysningen av den helikopterbaserte SAR-radaren PicoSAR og dens produserte refleksjoner fra terrenget. Bildene fra PicoSAR og det bistatiske oppsettet blir så sammenlignet og diskutert. Videre blir det bistatisk genererte bildet forbedret ved hjelp av en ulineær dopplerskift kompensering, hvor dopplerendringene gitt den bistatiske konfigurasjonen blir ivaretatt.

Masteravhandlingen er i sin helhet vedlagt i appendiks A.

Appendix A Masteravhandling

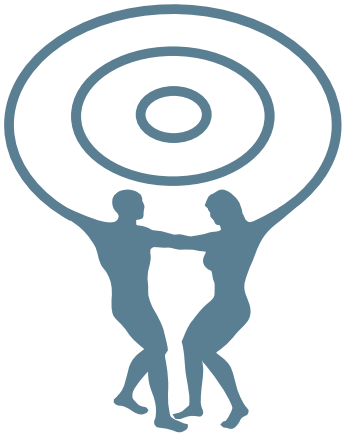

Høgskolen
i Narvik

SHO 6267

Master of Science in Technology

Bistatic SAR System with Stationary Receiver

Georg G Strømsmo

June, 2012

Department of Technology
Narvik University College

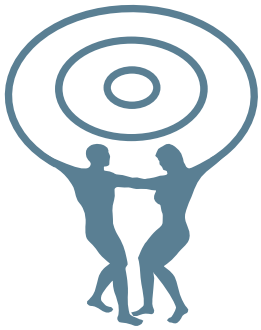

Høgskolen
i Narvik

Title:
Bistatic SAR System with Stationary Receiver

Author:
Georg G Strømsmo

Department:
Department of Technology

Supervisors:
Øyvind Thingsrud (FFI)
Stein Kristoffersen (FFI)
Raymond Kristiansen (HiN)

Principal:
Norwegian Defense Research Establishment (FFI)

Principal contact:
Øyvind Thingsrud (FFI)

Date: 1. July 2012

Classification: Open

Pages: 60

Attachments: 3

Keywords:
Synthetic Aperture Radar - SAR, Matched filter, Non Linear Chirp Scaling - NLCS, bistatic, Doppler effect,

Department of Technology
Narvik University College

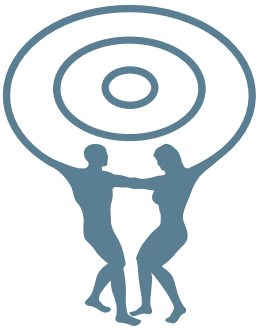

Høgskolen
i Narvik

Abstract

Abstract (English): This Master thesis takes the challenges of hitchhiking bistatic radar in fragments, investigate them, and use the solution to perform a bistatic imaging experiment. The transmitter were an airborne SAR and a fixed ground based receiver generate an image. There is no synchronization between the transmitter and the receiver other than the direct pulse.

The theoretical aspect for traditional monostatic SAR is presented in detail, and a bistatic adaption of this theory is made.

The image that is generated is enhanced with a Non Linear Chirp Scaling compensation, and compared to the airborne SAR's image and an uncompensated image. The experiment shows that bistatic SAR imaging is feasible, and describes further work.

Scenarios where the bistatic would be favored are described based on tactics and physical limitations.

Sammendrag (Norwergian text): Denne masteroppgaven tar for seg utfordringene ved en haikende bistatisk radar. Disse utfordringene deles opp, defineres, og taes hensyn til i et bistatisk avbildningseksperiment. Under eksperimentet fungerer en helikopterbåren SAR som sender, mens en fastmontert mottaker på bakken genererer bildet. Det er ingen synkronisering mellom sender og mottaker utover radarpulsene.

Det teoretiske aspektet rundt en trandisjonel avbildende radar blir beskrevet i detalj, og en bistatisk tilpassning blir gjort.

Bildet som er generert av det bistatiske systemet er forbedret gjennom en ulineær Dopplerskift kompensering. Bildet blir videre sammeliknet med det opprinnelige bildet som er tatt av den avbildende radaren i helikopteret, samt et bildet der ingen kompensering er blitt gjort.

Senario hvor det bistatiske systemet ville vært fordelaktig er beskrevet ut i fra taktikk of fysiske forutsetninger.

Department of Technology
Narvik University College

Preface

From the time where the Range-Doppler processing were carried out by optical prism, elaborated in [32], such as the SEASAT, to the modern approach with the Magellan Mission of Venus and the Shuttle Radar Topography Mission (SRTM) of the Earth, Synthetic Aperture Radar (SAR) technology has had a tremendous development the last decade. The modern Digital Signal Processing (DSP) and digital implementation made this development possible.

Today's radars have great computer capacity which gives the developer the ability to implement more sophisticated algorithms, and implement more hardware. Antennas with different polarization can be added to reveal more information about the surface. Moving beam makes the system able to have spot-mode which increases the integration time for azimuth resolution without using moving parts in space. And a system like TerraSAR-X along with its twin TanDEM-X which uses two separate satellites to perform interferometric mapping. Interferometry and polarimetry is probably two of the things that represent the development of SAR imaging in the early 2100-century. However, the old bottleneck of memory and down-link limitation still applies[1].

One of the next steps is to build bistatic and multistatic systems where the costly RF-transmitter unit may be left on a safe distance in a war scenario, while several Unmanned Aerial Vehicles (UAV) are deployed with receivers near the conflict without exposing its position. Another scenario where a bistatic or multistatic system might be preferred is when the transmitter is launched to space, with the receivers placed around the area of interest, fixed or on moving platforms. The image from the system can be processed and presented "immediately". For a advanced system, the receiver would not need a dedicated transmitter. Anything transmitting signals in the frequency-band that is fitted for the receiver antenna, filters, and bandwidth of the Analog to Digital Converter (ADC) could be used to generate an image of the surroundings.

The fact that bistatic and multistatic radar system are still not a mature science, I was motivated to write my thesis around these systems challenges. As my job in the Royal Norwegian Air force is airborne radar systems, these challenges are considered as highly relevant and interesting for me. Hopefully, this thesis will illuminate basic challenges with bistatic SAR system, and give a foundation for the decision whether bistatic SAR system should be a priority for Norwegian Defense Research Establishment (FFI) or not.

[1] TerraSAR-X can cover 400,000 square km for each revolution of the Earth with the lowest resolution 16m x 16m — 0.0078% of the surface. [http://www.gisdevelopment.net/application/casestudy/mi08_65.htm (June 2012)]

Acknowledgment

The EW-department at FFI deserve great acknowledgment as they built HEL, gave me an office with computers and software, tons of coffee, and always had time to enlighten dark corners. A special thank you goes to my supervisors Øyvind Thingsrud and Stein Kristoffersen that really made this six months a fun and interesting time. My third supervisor, Raymond Kristiansen, has been a good support and great representative for the University Collage in Narvik. He's been thorough, clear and motivating in all his feedback. And I hope I'll have the chance to work more with him at another occasion. Last, but not least, Chatrin, my better half, that had put up with me — or my absence — at the end of this work.

Georg G Strømsmo, Kjeller 2012

Contents

Abstract **iii**

Preface **v**

1 Introduction **1**

1.1 Problem 1

1.2 Scope and Thesis Objectives 1

1.3 Previous Work 1

1.4 Thesis Organization 2

2 Signal model **3**

2.1 Basic understanding 3

2.2 Doppler effect 5

2.3 Signal computation 6

2.4 Matched filter 8

3 Monostatic SAR **9**

3.1 Introduction 10

3.2 Geometry 10

3.3 Two Dimensional Signal $s(\tau,\eta)$ 11

3.3.1 Range (τ) 12

3.3.2 Cross Range (η) 13

3.3.3 Raw data array 14

3.4 Distortion 15

3.4.1 Topographical distortion 15

3.4.2 Earth curvature 16

3.4.3 Multipath 16

3.5 Limitation and usage 16

4 Bistatic SAR **19**

4.1 Introduction 19

4.2 Geometry 20

4.3 Two dimensional Signal $s(\tau,\eta)$ 21

4.3.1 Range (τ) 22

4.3.2 Cross Range (η) 23

4.3.3 Raw data array 23

4.4 Distortion 24

4.5 Limitation and usage 24

5 Experiment **27**
5.1 Introduction . . . 28
5.1.1 The Scene . . . 29
5.1.2 HEL - Hardware . . . 30
5.1.3 PicoSAR . . . 30
5.2 Hardware setup and limitations . . . 31
5.3 Software . . . 31
5.3.1 Echo raw data . . . 31
5.3.2 Direct pulse . . . 31
5.3.3 Transmitter parameters . . . 32
5.3.4 Geometrical parameters . . . 32
5.3.5 Range Compression . . . 32
5.3.6 Azimuth compression . . . 32
5.4 Expected results . . . 32
5.5 Measured results . . . 33
5.5.1 Result One, Figure 24 . . . 33
5.5.2 Result Two, Figure 25 . . . 34
5.5.3 Image Analysis . . . 35
5.6 Conclusion . . . 35

6 Conclusion and Future Work **37**
6.1 Conclusion of the experiment . . . 37
6.2 Future work . . . 37
6.2.1 Slave receiver for space borne transmitter . . . 38
6.2.2 HEL as a autonomous stand alone imaging system . . . 38

A Elaboration of Functions **39**
A.1 Ideal target function . . . 39
A.2 Fourier transform of a function . . . 39

B Matlab functions **40**
B.1 Distance between two GEO points . . . 40
B.2 Raw data readout and range compression . . . 40
B.3 Azimuth compression with no chirp focus . . . 41
B.4 Azimuth compression with NLCS . . . 41

C List of Acronyms **43**

D List of Symbols **45**

List of Figures

1 Complex signal Model . . . 3
2 Doppler shift $d\psi$ of f_{Rx} . . . 4
3 Doppler frequency distribution of moving platform . . . 5
4 Matched filter of a Chirped pulse . . . 8
5 Airborne monostatic SAR . . . 9
6 ISO range and Doppler for a monostatic SAR system . . . 11
7 Monostatic ground range signature of point scatterer A . . . 12
8 Azimuth compression of point scatterer A, B, and C . . . 13
9 Doppler and Slant-range signature for point scatterer A, B, and C . . . 14
10 Topographical distortion . . . 15
11 Single- and double-bounce multipath . . . 16
12 Bistatic SAR system with airborne transmitter and fixed receiver . . . 19
13 Geometry for bistatic configuration . . . 20
14 ISO Range and Doppler for bistatic configuration with fixed receiver . . . 21
15 Bistatic ground range signature of point scatterer A . . . 22
16 Azimuth compression of point scatterer A, B, and C . . . 23
17 Doppler and Slant range signature for Point scatterer A, B, and C . . . 24
18 EKKO II trailer and the FFI Science team . . . 27
19 Practical Test Environment . . . 28
20 Optical image of the Scene, downloaded from www.finn.no . . . 29
21 Sketch of HEL's components . . . 30
22 HEL software functional block diagram . . . 31
23 SAR image made by the PicoSAR . . . 33
24 Result One: HEL-image without Chirp Scaling . . . 34
25 Result Two: HEL-image with Chirp Scaling . . . 34
26 Comparison of Result One and Result Two . . . 35
27 Appendix: Ideal Target Function . . . 39
28 Appendix: Fourier transform . . . 39

1 Introduction

1.1 Problem

This work has been given the challenge to adapt a receiver to *hitchhike* on a monostatic SAR imaging scenario. The primary goal is to build a theoretical foundation around the differences between the monostatic and the bistatic geometry, such as geometrical distortion and limitation and imaging algorithms that can be adapted to a bistatic system. This foundation should be used to optimize and explain the factors around a bistatic SAR experiment.

The usage of bistatic systems should be explained, and benefits compared to a monostatic system pointed out.

Theoretical statements should be confirmed with simulations to verify dynamics, and visualize the difference between a well defined monostatic system and a nontraditional bistatic approach.

An experiment should prove statements, simulations, and motivations around the thesis.

1.2 Scope and Thesis Objectives

The thesis will investigate the Non Linear Chirp Scaling (NLCS) algorithm for SAR imaging based on the work in [6], [37], and [18], where this algorithm is considered as an innovative and effective way to adjust the data to focus for a bistatic scenario. Other algorithms may be presented but not elaborated.

Necessary knowledge of signal theory and geometrical parameters will be described and simulated.

The scenario used for simulation and field data will be based on a moving transmitter with no *squint angle* and a stationary receiver. These conditions are necessary for the NLCS-algorithm to be optimal in a bistatic geometrical setup where computation load should be kept at a minimum [18].

1.3 Previous Work

Bistatic SAR-systems are still in its cradle. Many scientists have established great theoretical foundation, such as *Processing Algorithms for bistatic Synthetic Aperture Radar Data* written by Neo Yew Lam in 2010 [18], also EUSAR 2010 and EUSAR 2012 published a great amount of papers touching these problems [7][4][12][25][20]. The twins, TerraSAR-X and TanDEM-X, are an up and running bistatic system, where these two satellites flies in a helix formation performing interferometric measurement to improve high accuracy [11][4][17][28]. However, few bistatic commercial system exist.

SABRINA - SAr bistatic fixed Receiver for INterferometric Application, made at Universitat Politècnica de Catalunya (UPC), is a two channels Radio Frequency (RF) receiver made for ENVISAT and ERS-2 transmitter described in [30], [9] and [7]. It has the ability to record the reference pulse directly from the transmitter and into memory in the same time as it record the back-scatterer from the scene. This give the system a reference-pulse for each back-scatterer signal for the range compression sequence.

HITCHHIKER is a receiver also made for the bistatic SAR geometry, and described in [6]. HITCHHIKER was made in 2009 by the Center for Sensor systems at the University of Siegen.

Unlike SABRINA, it uses the direct signal from satellite as a trigger as well as the reference for range compression. The other receiver records the back-scatterer from scene when it's triggered by the first receiver. This reduces expensive memory usage.

HEL - Hitchhiking Echo Location, is a system made at FFI, which has the same ability as HITCHHIKER, also tuned in for X-band transmitter such as the TerraSAR-X and PicoSAR — described later in this paper. HEL were built before this thesis, but the image processed in this thesis were the first raw data set HEL generated.

1.4 Thesis Organization

Chapter One introduces the thesis, and the process around it. Previous Work shows that other project that have been successful in their attempt to try the concept.

A whole chapter has been dedicated to present the signal model in Chapter Two. This is mainly due to the complexity of a simple effect — the Doppler effect. In Chapter Three, monostatic SAR system is presented, with all the components that are transferable to a bistatic system. With the same approach used to the monostatic system, the bistatic system is presented in Chapter Four.

Chapter Five gives a presentation of the process and the outcome of a practical test of the HEL which hitchhike on the monostatic SAR system PicoSAR.

Finally, Chapter Six present a conclusion and evaluation of the system, and what could be the next step in the manner of future work.

In the Appendix, the elaboration of function that are used in this thesis are given. Also, Matlab functions that were made exclusively for this thesis are given here.

2 Signal model

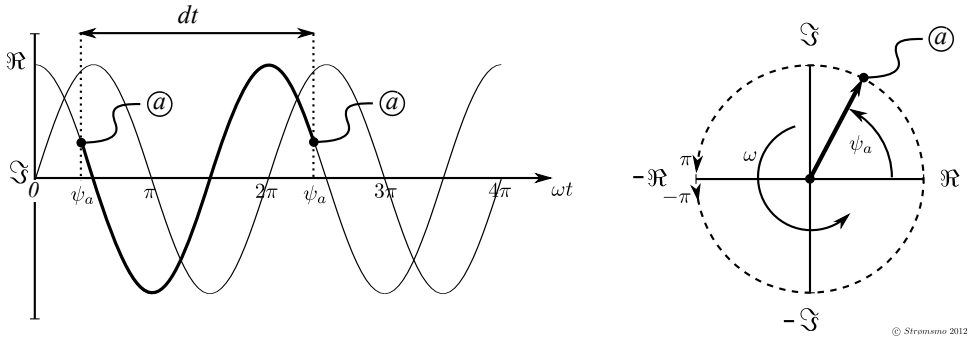

Figure 1: Complex signal Model

This chapter describes the properties of a signal that is crucial to understand further in this thesis. The electromagnetic wave's electrical part is broken down in mathematical expression so the influence on physical — both spatial and electromagnetic — factors can be described, calculated, and estimated.

2.1 Basic understanding

Monostatic and bistatic SAR systems process with complex presentation of sine signals. This section will present terms and notations of signal types concerning SAR systems.

Frequency is the measurement for a periodic signal to repeat. A heartbeat have a rhythm with a given frequency. A color also have a frequency [38]. White noise, on the other hand, can not be defined by a repetition sequence, and can not be described as a single frequency. In radar signal, the frequency is given in repetition per second, called Hertz[2], and noted Hz $\left[s^{-1}\right]$. For air and space borne applications X-band is often used[3], which spans from $8GHz$ to $12GHz$ [1]. Frequency f can be found by measure the time it takes to perform one cycle, as illustrated in Figure 1.

$$f = \frac{1\ cycle}{dt} \tag{1}$$

A frequency's *wavelength* λ is a function of the frequency f and the medium that the electromagnetic wave travels through. The microwave's length in meters to perform one cycle defines the wavelength. In the case of vacuum, such as in space, the electromagnetic wave travels with the speed of light[4] c and the length is.

$$\lambda = \frac{c}{f}\ [m]. \tag{2}$$

The *Phase* ψ of a frequency goes from $-\pi$ to π. The phase to point a in Figure 1 is called ψ_a and illustrated by an arrow. As time goes, this arrow rotates counterclockwise with the velocity of angular frequency

$$\psi = 2\pi ft\ [rad]. \tag{3}$$

$$= \omega t \tag{4}$$

[2]Named after the German Heinrich Rudolf Hertz (1857–1894)

[3]Because the wavelength is short, waveguides, amplifiers, and antennas are kept small and light

[4]In this thesis, all electromagnetic waves are considered to travel with the speed of light.

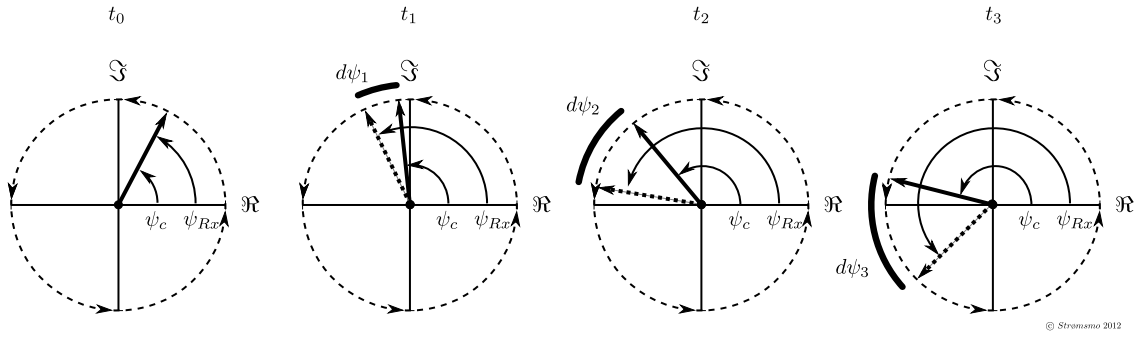

Figure 2: Doppler shift $d\psi$ of f_{Rx}

Angular frequency ω is a presentation of a frequency in the manner of it's phase variation over time, radians per second. Figure 1 shows an arrow pointing at point a. The arrow, which rotates counterclockwise as times goes, will come to the same point after a rotation of 2π after $t = \frac{1}{f}$ seconds. I.e. if the frequency is one Hz, the time is one second. If the frequency is $9GHz$ the time is 1.111×10^{-10} second, or 111.1 picoseconds.

$$\omega_0 = 2\pi f_0 \tag{5}$$
$$= \frac{2\pi}{s} \left[\frac{rad}{s}\right] \tag{6}$$

The factor between phase and angular frequency is the instant time. If the phase at time t_0 is zero and the phase at time t_a is ψ_a, then the angular frequency is

$$\omega = \frac{d\psi}{dt} \tag{7}$$
$$= \frac{\psi_a - 0}{t_a - 0} \tag{8}$$

Chirp is the term used for a frequency that varies — a frequency modulation. This thesis only handle linear modulation, which is referred to as Linear Frequency Modulation (LFM) [34][18]. Consider an amplitude function of time $a(t)$ that is one when $0 < t \leq T$, and zero elsewhere. A chirp like $\cos\left(\omega_c t^2\right)$ will have a start frequency equal zero and stop frequency of $2T\omega_c = Tf_c/\pi$ [34] — an up chirp. Hence,

$$Up\ chirp = a(t)\cos\left(\omega_c t^2\right) \tag{9}$$
$$Down\ chirp = a(t)\cos\left(-\omega_c t^2\right) \tag{10}$$

The component ω_c is known as the *chirp rate*.

Doppler effect[5], both Doppler shift $d\psi$ and Doppler frequency f_d, is generated by spatial movement — the Doppler effect makes an ambulance change tone as it passes. The Doppler effect is a deviation. E.g. in Figure 2 there are two phases illustrated, one without Doppler shift ψ_0 and one with ψ_{Rx}. If ψ_{Rx} is the received echo of the sent ψ_0, then $d\psi_1$would represent the Doppler deviation from t_0 to t_1, and $d\psi_3$ would represent the Doppler deviation from t_0 to t_3.

[5]Named after the Austrian physicist Christian Doppler (1803–1853)

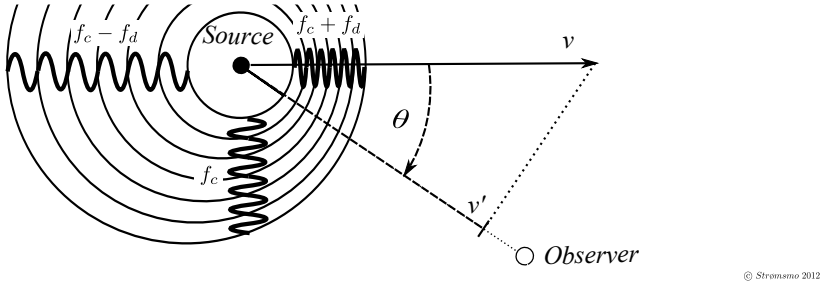

Figure 3: Doppler frequency distribution of moving platform

2.2 Doppler effect

The understanding of Doppler effect is crucial in SAR imaging, and this section will describe the phenomenon even further. It is basically just a change in spatial condition for the instant phase.

Consider a ball floating in water which is moved up and down. Waves are distributed 360° around the ball with a frequency equal the rhythm of the ball. If the ball are moved while it makes these waves, the wave in front will have a higher frequency, shorter wavelength, that the rhythm of the ball would imply. The wave in the back have the same difference, but negative. Waves that are sent perpendicular to the moving direction have the same frequency as before. In front of the ball, Doppler frequency is added to the original frequency, while the frequency behind the ball are subtracted the Doppler frequency, shown in Figure 3.

Example, if the measurement of a receiver, who have an ADC for both f_c and f_{Rx}, is;

	ψ_0	ψ_{Rx}
t_0	1.04700000	1.04700000
t_1	1.65800000	1.65800005
t_2	2.26900000	2.26900010
t_3	2.88000000	2.88000015

The sampling rate of the ADC is 10^8 samples per second, would give an $f_0 = 9\,724\,367\,022.9148Hz$ and $f_{Rx} = 9\,724\,367\,818.689522Hz$, based on (7) and (5). From the readout table, the deviation between the two readouts are 0.5×10^{-7} for every sample. This means that the Doppler shift of 0.5×10^{-7} radians every 10th picoseconds should correspond to a Doppler frequency of $795.77Hz$. This is also the difference between f_{Rx} and f_0.

If this radar were operated by a Police man, pointing towards a car that is heading his way, the speed measurement of the radar would be [38]

$$\begin{aligned} f_d &= f_0 \frac{v}{c} \\ &\downarrow \\ v &= \frac{f_d c}{f_0} \\ &= \frac{795.77Hz \cdot 3 \times 10^8 \frac{m}{s}}{9\,724\,367\,022.9148Hz} \\ &= 24.55 \frac{m}{s} \\ &\approx \underline{88.4km/t} \end{aligned}$$

In the case were there is an offset θ, illustrated in Figure 3, angle between Line Of Sight (LOS) from the policeman to the car and the velocity vector of the car, the speed measurement will only give the radial velocity.

$$f_d = f_0 \frac{v}{c} \cos\theta \tag{11}$$

The Doppler effect that an observer experience when an ambulance passes will have a θ that varies from zero to 180 degrees if the observer walk on the side of the road in the opposite direction as the ambulance — such that they meet and passes. The sound of the siren will have a frequency modulation where the start frequency is siren plus Doppler shift, and the end frequency is siren minus Doppler shift. In the split second where it passes, the chirp can be simplified to a LFM. When the observer is moved further from the road, the chirp rate decreases in that split second.

Doppler centroid is at the direction where the Doppler effect changes polarity, or in the instant time where Doppler is equal zero, i.e. $\theta = 90^\circ$ [23]. In figure 6, Doppler centroid are the lines perpendicular to the flight direction. One on the left, and one on the right side.

2.3 Signal computation

In this thesis, computation of signals are mainly given as exponential function — the *Euler formula*[6], defined as [38]

$$e^{j\psi} = \cos\psi + j\sin\psi. \tag{12}$$

For a continuous signal where $\psi = \omega t$ from (4), the formula becomes

$$e^{j\omega t} = \cos\omega t + j\sin\omega t \tag{13}$$

Where t is the time elapsed, ω is the angular frequency of the given signal and j is the imaginary unit. This presentation of the signal gives a real part, and an imaginary part which is delayed with 90°degree compare to the real part. In radar science, these to components are referred to as the *In Phase Channel* for the real part and the *Quadratic Phase Channel* for the imaginary part, I Channel and Q Channel, respectively [32].

The mixing, or multiplication, $p(t)$ of two sine signal f_1 and f_2 can be by combine their exponential presentation,

$$\begin{aligned} p(t) &= e^{j2\pi f_1 t} \cdot e^{j2\pi f_2 t} \\ &= e^{j\omega_1 t} \cdot e^{j\omega_2 t} \\ &= e^{j\omega_1 t + j\omega_2 t} \\ &= e^{j(\omega_1+\omega_2)t}. \end{aligned}$$

If the signal is pulsed with an amplitude $a(t)$ which is one for $0 < t \leq T$ and zero else, the received signal becomes

$$p(t) = a(t)e^{j(\omega_1+\omega_2)t}. \tag{14}$$

Combination of signal does not have to be of two continuous sine signal. In FM radio transmission, ω_1 could be the carrier frequency of e.g. 92MHz, while the host's voice is represented by ω_2. The

[6] Named after the Swiss Leonhard Euler (1707–1783)

amplitude function $a(t)$ would then be the combination of the carrier frequency strength $a_1(t)$ and how loud the host talks $a_2(t)$. In mathematical form, the transmission $p(t)$ becomes

$$p(t) = [a_1(t) + a_2(t)]\, e^{j(\omega_1+\omega_2)t}.$$

A radio set tuned through the frequency band of FM broadcasting, and stopped at a frequency f_{LO}, with angular frequency equal ω_1 and an amplitude equal $a_1(t)$, will be able to play this radio show. The frequency f_{LO} is subtracted by mixing from the received signal $s(t)$,

$$\begin{aligned} s(t) &= [a_1(t) + a_2(t)]\, e^{j(\omega_1+\omega_2-\omega_{LO})t} && (15)\\ &= a_2(t) e^{j\omega_2 t}. && (16) \end{aligned}$$

The result is the voice of the host alone. The frequency f_{LO} is the frequency of a Local Oscillator (LO) [32], shown in Figure 21. In radar design, where frequencies are in X-band, few Digital to Analog Converters (DAC) and ADC are able to sample with Nyquist rate[7], which is twice the frequency of the measured signal's frequency. For a signal of 9GHz, the sampling rate has to be 18 000 Mega Sample Pr Second (MSPS) to fulfill Nyquist criteria. Using local oscillator and mixers, high frequencies, often referred to as Radio Frequencies (RF), can be emitted out in the atmosphere with the benefit this gives, and Intermediate Frequencies (IF), can be used in signal recognition and DSP unit.

[7] Named after the American Harry Theodor Nyquist (1889–1976)

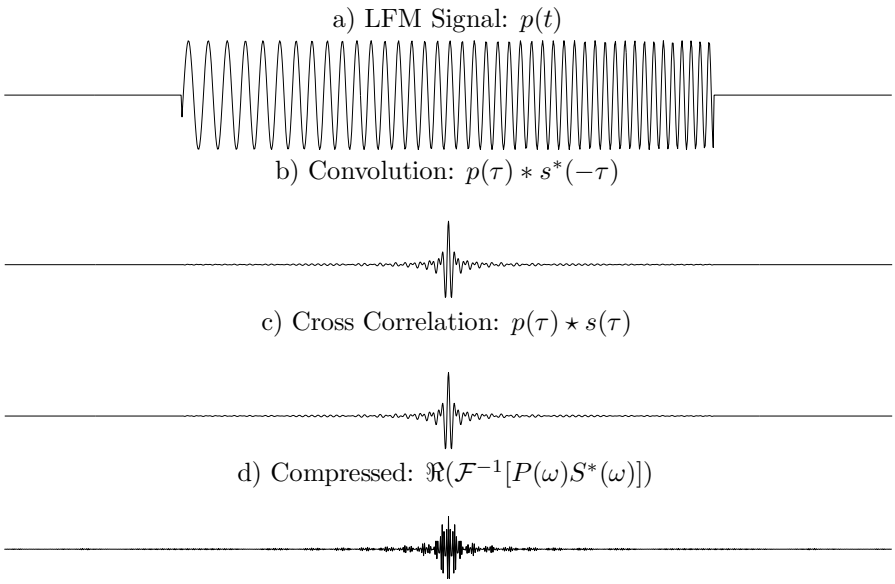

Figure 4: Matched filter of a Chirped pulse

2.4 Matched filter

Radars performance might be given by the spatial resolution. An infinite short pulse such as a Dirac delta function[8] would give a infinite range resolution. This is, however, not an optimal, nor feasible, option. A long pulse is desired. For a long pulse, large amount of energy are given to, and received from, a point scatterer while the energy strain on the radar is kept low. A long pulse will, though, make echoes overlap, and range resolution gets poor. A solution is range compression. By multiplying a LFM, such as (9) to an LO output, the transmitted signal $p(t)$ becomes

$$p(t) = a(t)e^{j(\omega_{LO}+\omega_c t)t}. \tag{17}$$

A matched filter uses a known reference, such as a copy of the transmitted signal, and performs a cross correlation between this known reference and received signal. The same result is achieved with the convolution of the received signal and the complex conjugate and time reversed of the reference signal. These two are, however, heavy to compute. Another approach is used where the two signal are Fourier transformed[9] and multiplied. The Fourier transform is explained in Appendix A.2. All three techniques are illustrated in Figure 4.

What is happening in a matched filter is that a correlation is integrated. If the pulse were a single sine, then the correlation would start to integrate when the first lambdas met, because they match. After a whole convolution, the output would be a triangle which are twice as wide as the pulse length, and the peak in the middle were the match were hundred percent. By changing the single sine to an LFM, a hundred percent match will only occur when pulses are directly on top, and non match elsewhere — as shown in Figure 4. A constant Doppler shift will move and reduce the match.

[8] Named after the physicist Paul Dirac

[9] Named after the french mathematician Jean Baptiste Joseph Fourier (1768–1830)

3 Monostatic SAR

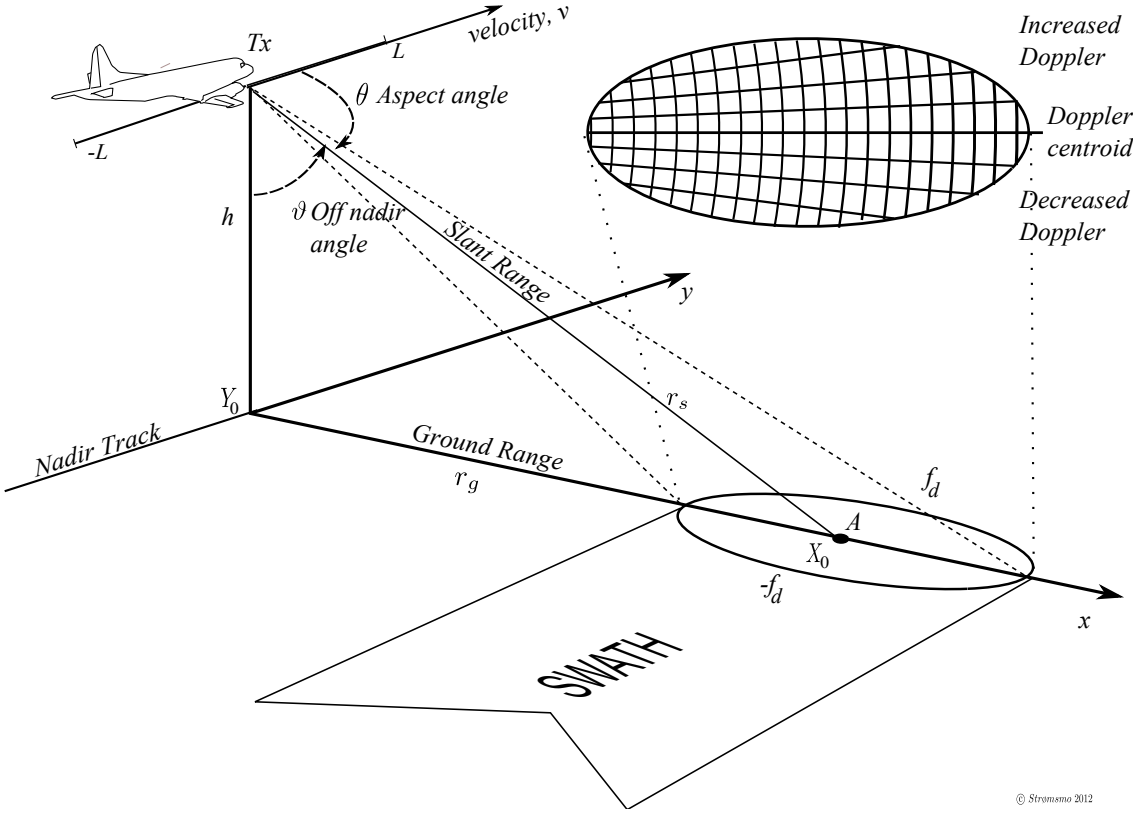

Figure 5: Airborne monostatic SAR

Side Looking Airborne Radar (SLAR) were the first imaging radar technique. The concept were a radar with an antenna pointing perpendicular to the flightpath. The antenna, with diameter equal D, had pulses with a carrier frequency of wavelength λ. Azimuth resolution for this systems is $\sim R\lambda/D$, where R is the range [33]. SLAR is a Real Aperture Radar (RAR), and has no ability to integrate echo's Doppler history. The resolution is at mercy of antenna diameter and frequency wavelength, which have their limitation in an aircraft or a satellite. Motorola AN/APS-94D is such a radar [35].

In 1952-1953, Carl A. Wiley developed *Doppler Radar Beam Sharpening* that were implemented in DOUSER [21][2]. This is known as *Doppler Beam Sharpening (DBS)* radars and found in radars such as AN/APG-66v2 on F-16 Fighting Falcon[10]. Such imaging technique can present an image, covering a large area, in approximately real time [27]. Broadside cross range resolution is $R\lambda/L_{DBS}$, where L_{DBS} is the synthetic aperture, i.e. from -L to L in Figure 5 [33].

The first SAR were unfocused — *Unfocused SAR*. The signal processing in these radars did, and do, not take in to account the changing azimuth chirp rate that occur in range. If this consideration is done, a fully operational range invariant imaging radar are designed — *Focused SAR*.

[10] http://www.northropgrumman.com/farnborough/briefings/assets/2010-fas-f-16-radars-briefing.pdf (May 2012)

3.1 Introduction

The main difference between a SAR and a RAR is the azimuth resolution handling. The RAR has a narrow main beam, or two main lobes for the monopulse-design or lobeswitch-design, to separate objects positioned in the same range. SAR, on the other hand, has a wide main lobe[11] in azimuth. The wide beam/lobe gives a longer Doppler shift-signature for each point scatterer. This Doppler component generated by the platform's movement is used to enhance the azimuth resolution. The product is a "range-invariant" azimuth resolution, and the price is decreased sensitivity - or Signal to Noise Ratio (SNR) [33].

For range resolution, the signal processing might be of the same kind. A LFM pulse can be compressed by cross correlation to a desired reference. This is performed by a *matched*-filter which is a convolution of the received signal $s(t)$ with a complex conjugate and time reversed copy of the sent pulse $p(t_0)$.

3.2 Geometry

The geometry of a SAR imaging scenario consists of the SAR platform, which can be an aircraft, satellite, car, train, UAV, and so on. Also a scene, with a scene center $(X_0,\ Y_0,\ 0)$. The scene in this thesis is referred to as the Region Of Interest (ROI).

The ROI consist of an infinite numbers of *point scatterers*. A point scatterer is anything that reflects the microwave that is sent by the transmitter. Point scatterers may be a car, soda can and even a hairpin. In most cases, point scatterers are smaller than a resolution cell of the radar system, and a cluster will act as one point scatterer. In some cases, where the image seems to have arbitrary speckle, like white Gaussian noise, the cluster of infinite point scatterers would have an unique signature. This fact makes it possible to distinguish objects with two pass interferometry.

The distance from the SAR platform and a given point scatterer is the slant range r_s. The slant range is given by the time the pulse travels forth and back with the speed of light. This time is divided by two due to the forth and back traveled distance. For an image to be displayed, this domain has a geometrical distortion which is corrected by knowing the altitude of the SAR platform with respect to the point scatterer, or ROI with flat Earth assumption;

$$r_g = \sqrt{r_s^2 - (h - h_{ROI})^2}. \tag{18}$$

As the SAR receiver uses the wave's propagation-velocity to calculate the range to a point scatterer, it also use the Doppler shift for that point scatterer. The Doppler shift is generated by the SAR-platform flightpath and velocity with respect to the point scatterer. This means that the raw data measured by the receiver is in a *slant-range domain*. Geometrical correction has to be done to convert the data from slant-range domain to *ground-range domain*. For airborne system the flat-Earth assumption and a local North - East - Down (NED) reference frame can be used to simplify geometrical computations for one imaging scenario. Platforms height and attitude have to be continuously monitored and corrected due to small variations and vibrations for an airborne platform. This is done by combining Global Positions System (GPS) position with an Inertial Measurement Unit (IMU) that deliver sufficient platform-movement data from pulse to pulse. For a system with Pulse Repetition Frequency (PRF) of 1kHz, the processing algorithm would need a >1kHz update rate from the navigation unit.

[11] In this Thesis *beam* refers to the transmitting sequence, and *lobe* to the receiving. I.e transmitter main beam and receiver main lobe. This corresponds to definitions given in [1] and [5].

Basically, the geometry can be referred to in the matter of an orthogonal right hand 3D-frame $[range,\ cross-range,\ altitude]$, similar to the one in Figure 5, as;

- Point A at Scene center; $A\,(X_0,\ Y_0,\ 0)$
- Platform position; $P_{Tx}\,(0,\ \eta v,\ h)$
- Slant-range;

$$r_s = \frac{\tau c}{2} \tag{19}$$

$$= \sqrt{(0-X_0)^2+(\eta v-Y_0)^2+(h-0)^2} \tag{20}$$

- Ground-range;

$$r_g = r_s \sin\vartheta \tag{21}$$

Where τ is the time for transmitted pulse to get forth and back from a point scatterer — later referred to as *fast time*, and η is the azimuth time — also referred to as *slow time*. $\eta v = -L$ is the beginning of the imaging scenario, and $\eta v = L$ is the end of the scenario. Platform velocity is v and ϑ is the Off Nadir angle.

3.3 Two Dimensional Signal $s(\tau,\eta)$

Rooted in the geometrical foundation given in the section above, the slow-time η refers to the azimuth axis, and the fast-time τ refers to the range axis of a signal array. This signal-domain data has to be converted to a spatial image-domain; range and cross range. Figure 6 illustrates the effect that SAR-algorithms process. The circles around the arrow illustrated the range cells. Each circle has a constant range to the transmitter/receiver. The straight line perpendicular to the arrow is where the Doppler effect is zero. The Doppler shift increases for every line in front of that line and negative Doppler shift increases for every line behind the line perpendicular to the arrow. Maximum Doppler effect appear in front of and behind the arrow.

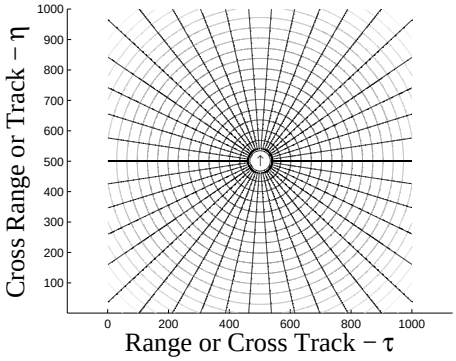

Figure 6: ISO range and Doppler for a monostatic SAR system

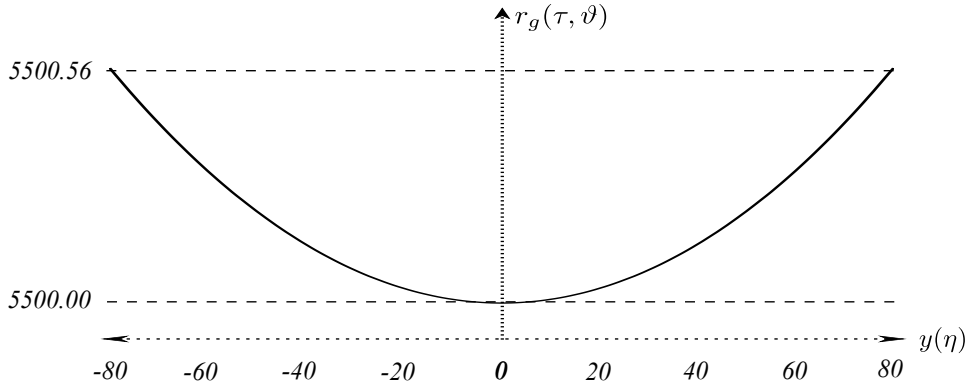

Figure 7: Monostatic ground range signature of point scatterer A

3.3.1 Range (τ)

The first step in ranging is to range compress the received signal for each pulse. This is done by cross correlate the raw data signal with a desired reference. A replica of the transmitted pulse can be used. Range compression is done with matched filter, described in 2.4.

With a known sampling rate of the ADCs, each sampled value correspond to an elapsed time. With a sampling rate of 500 MSPS, each 500 sample represent one microsecond. Each microsecond represent 150 meter in slant range.

For the Earth atmosphere, microwave travels with approximately the speed of light in vacuum c. Ranging, slant range r_s, for the radar is found by timing a pulse from when it is sent to time it is received as an echo. Due to the forth and back propagation of the pulse, the slant range has to be multiplied with two, as mentioned in the geometry section. The round-trip time τ_n for point scatterer n is found by

$$\tau_n = \frac{2r_{s_n}}{c}. \tag{22}$$

$$r_{s_n} = \frac{\tau_n c}{2} \tag{23}$$

This ranging is in the slant range domain, and conversion to ground range is done by one of the functions (18) or (20).

$$r_{g_n} = \sqrt{r_{s_n}^2 - (h_{Tx} - h_n)^2}, \tag{24}$$

$$r_{g_n} = r_{s_n} \sin\vartheta_n \tag{25}$$

where ϑ_n is the off nadir angle to point scatterer n, and h_n is the height of that same point scatterer. In Figure 7, the plot of ground range signature of point scatterer A. The closest point is 5,5km from nadir track, which is the actual distance for point scatterer A to the nadir track. The hyperbola in Figure 7, the longest range to point scatterer A is 5500.56 meters. It the range cell spans over 30cm, energy of the point scatterer will end up in the wrong range cell, and degrade azimuth compression, explained and simulated in the next sub section.

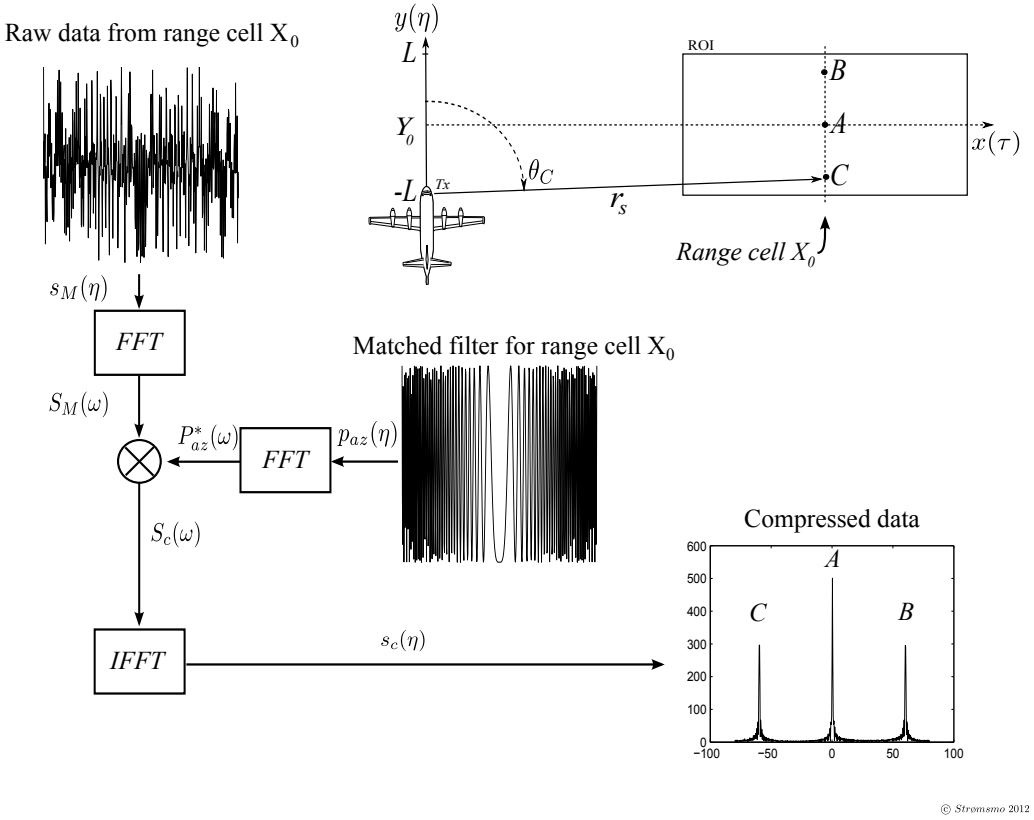

Figure 8: Azimuth compression of point scatterer A, B, and C

3.3.2 Cross Range (η)

Cross ranging uses the Doppler frequency ω_d that is generated by the movement of the SAR platform over time t. This azimuth chirp can be predicted by the geometrical function

$$\omega_{dc} = \omega_0 \frac{v}{c} \cos\theta_C. \tag{26}$$

Where θ_C is the aspect angle to point scatterer C, illustrated in Figure 8, and ω_0 is the sent frequency of the SAR.

A matched filter built with (26) will compress all point scatterers with Doppler signature that matches that range.

In Figure 8, three point scatterers A, B, and C, are places at the same distance X_0 to nadir track. Their azimuth chips are summarized into a vector called *Raw data from range cell* X_0. Both, matched filter and the raw data vector are transformed to wave domain. The filter is time reversed and complex conjugated. The two Fourier transformed signals are multiplied and inverse transformed. This gives a azimuth compressed signal $s_M(\eta)$ were the reflected energy from A, B, and C are placed correctly. Point scatterers B and C have lower peak power than A, this is due to the correlation of the filter and the signature. Point scatterer A have 100% overlap, while B and C have approximately 75% correlation overlap.

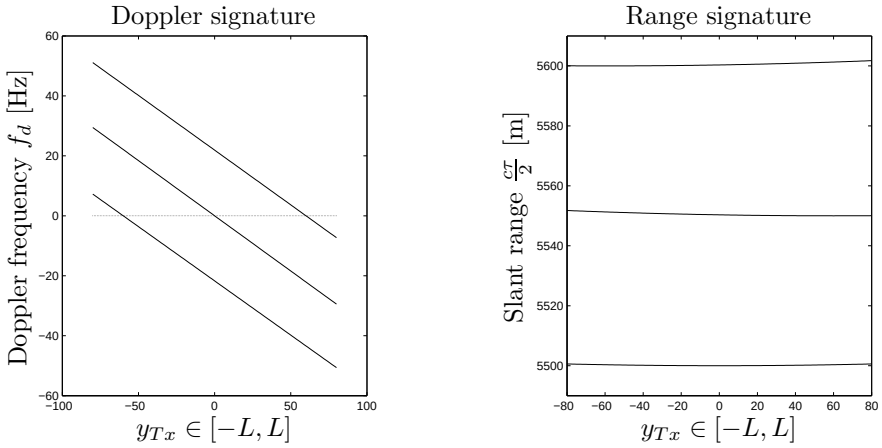

Figure 9: Doppler and Slant-range signature for point scatterer A, B, and C

3.3.3 Raw data array

For a scenario where there are three point scatterers *A*, *B*, and *C* placed in a local coordinate-frame along with the transmitter/receiver *Tx*, where;

- $Tx(0,\ \eta v \in [-L, L],\ 1km)$,
- $A(5.5km,\ 0,\ 0)$,
- $B(5.55km,\ 60m,\ 0)$,
- $C(5.6km,\ -60m,\ 0)$.
- $f_0 = 9.65GHz$

Consider the velocity $v = 32m/s$ and synthetic aperture $L = 80m$. As given in the first pullet point, the SAR platform flies with a constant altitude of $1km$ and a constant velocity of $32m/s$. The imaging sequence starts at $y_{Tx} = -80$ and ends when the radar is at $y_{Tx} = 80$, i.e. an integration time of $\frac{160m}{32\frac{m}{s}} = 5$ seconds.

Figure 9 shows the signature the imaging processor can use to distinguish and place the point scatterers. In the Doppler signature plot, the point where the graph for each point scatterers crosses zero, which is the horizontal line, correspond to its *y* element in the local coordinate frame — azimuth in the image. The other plot, shows the slant range for each point scatterer. The nearest point to the flightpath of the SAR for each point scatterer is the *y* element for that point scatterer. Also the highest σ will occur at that point. After range compression, the Doppler info can be used to compress the signature that is smeared out in azimuth.

The slope of the Doppler signature to e.g. point scatterer A, the one that crosses zero Doppler when $y_{Tx}$is equal zero, represent an azimuth chirp. In that case, the start frequency ω_0 is 30Hz and the chirp rate ω_c is $\frac{df_d}{dt} = \frac{60Hz}{5s} = 12 \rightarrow \omega_c = 2\pi \cdot 12$. Hence, azimuth compression to this raw data could be carried out with a reference pulse equal

$$p(t) = a(t)\exp(j2\pi \cdot 30t - j2\pi \cdot 12t^2) \qquad t \in [0,\ 5]. \tag{27}$$

Because these three targets are close to each other, the chirp rate remains approximately the same. Hence, the same reference pulse can be used for all three point scatterers. The result will be, after convolution, an azimuth compression as shown in Figure 4.

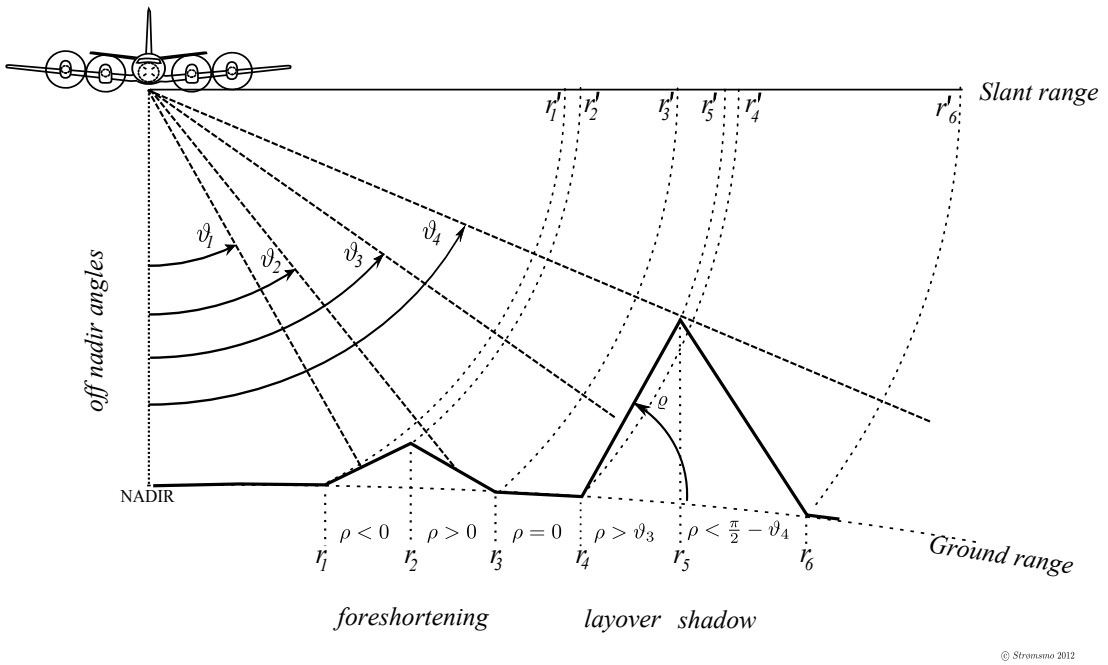

Figure 10: Topographical distortion

For a monostatic SAR algorithm, such as Chirp Scaling Algorithm (CSA), each range cell would be compressed by using a predicted reference pulse to fit the chirp expected for that slant range. One for range cell X_0 in Figure 8, and a different for the next range cell $X_0 + \delta x$.

3.4 Distortion

SAR imaging suffers from distortions. This is generated by the topography, Earth curvature, Earth oblateness, and scenario slant-range hyperbola.

3.4.1 Topographical distortion

Topographical distortion are separated in three types, all shown in Figure 10. At foreshortening image is either compressed or stretched, while the more destructive types; layover and shadowing rearrange or has no information, respectively.

Foreshortening refers to the effect that occur when the terrain has an offset angle ρ compare to the assumption of a flat Earth. If the angle is positive, with counterclockwise as the positive direction of rotation, the foreshortening effect results in a compressed area in the slant-range domain. This effect is represented by r'_1 and r'_2, which is closer than their origin in ground-range domain — represented by r_1 and r_2. In the opposite case, where the angle ρ is negative, the area get stretched — illustrated by r'_2 and r'_3.

Layover, represented by point r'_5 and r'_4, is when ρ is greater that the off nadir angle ϑ. Point scatterers further out in the scene appear closer in slant range. For shadowing, where ρ is less than $\frac{\pi}{2} - \vartheta$, the topography makes it impossible to get illumination from the transmitter to the scene, and echo from the scene to the receiver.

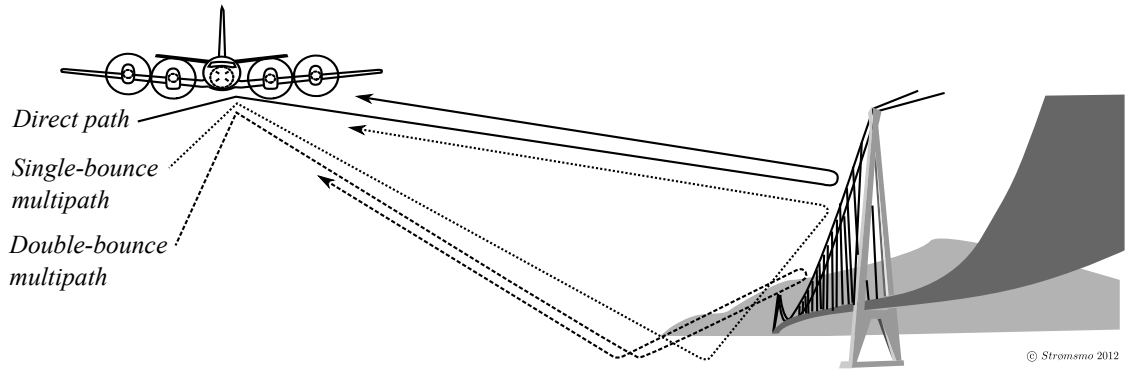

Figure 11: Single- and double-bounce multipath

Layover and shadowing contains information even though they might occur as limitations. The shadow of a building would represent its height, and the layover of a large ship at the sea-surface would represent the vessel's vertical side pointing towards the receiver. Even layover from a vessel, at the ground can be extracted from the echos from ground by two-pass interferometric imaging, where as the vessel's echos would change due to ocean waves. Although, interferometric imaging is not covered by this thesis.

3.4.2 Earth curvature

Earth curvature contributes to a non linear change in ground resolution. For space born application, where the swath is wide, this factor has to be corrected. In airborne SAR-imaging, the Earth might be considered as flat[12] due to the narrow swath width compared to the Earth curvature.

3.4.3 Multipath

Multipath is when the transmitted pulse does not take the shortest path, the path that would give the time delay that correspond to the slant-range in the calculation. As illustrated in Figure 11, a single-bounce multipath of the signal would lead to a imaging of the same bridge a bit further away that the direct path pulse would represent. And the double-bounce multipath would make the processor draw up a third bridge in the image [14][16][19].

3.5 Limitation and usage

In Figure 6, the sectors optimal for SAR imaging do not cover all directions. The optimal sectors are those who points perpendicular to the flight path.

Shadowing and overlay, as shown in Figure 10, do also give boundaries. A off nadir angle of 45° is a good compromise between these two limitations. In areas like Norwegian fjords, with high and steep mountains, overlay and shadowing effect the way the SAR platform has to be maneuvered.

The usage of monostatic SAR systems to day is e.g. ice melting surveillance, where a space borne SAR platform can collect image data of a large area, and compare to earlier data to reveal changes. Sea ice classification where the amount of ice can be calculated and thereby the amount

[12] Statement by Gregory Sadowy from Jet Propulsion Laboratory, USA at the EUSAR 2012 Conference

of freshwater captured in the ice. Also passage mapping for ships [10], where thin or broken ice can be found to create a safe path for vessels.

At sea, the surface are usually uneven because of the waves, specially ripple waves. If oil spill are located at the sea surface, a SAR image of that spill will give a good representation of the spill because the ripples are reduced [3]. Ripples gives diffuse echos where some energy always will go in the direction of the receiver. When ripples are reduced, diffuse scattering are reduces and there will be specular scattering insted. These echoes does not go back to the receiver, and the area becomes black, like shadows.

For flooded area, a space borne SAR can give data to predict and calculate destruction [22][29] which give valuable information for damage minimizing.

The benefit of space borne synthetic aperture radars is that large areas can be covered with a low cost, and data can be compared with the frequency of the revisiting time, for low earth orbit satellites, revisiting time is approximately 11 days [31]. This is also a problem for some applications where update frequency has to be higher than 11 days. Or that the data has to be collected faster. For space borne systems, the satellite has to pass through a down link[13] sector to send imaging data to, which transfer the data to the desired location.

Air borne SAR systems can be deployed at a position and stay there for continuously update of imaging. The collected data are already in the sector of a down link, so images are available almost instantly. This capacity might be preferred in a conflict area, forest fire, earthquake and tsunami.

A SAR can deliver images even when it's dark, or if the visibility is poor. The radar does not need illumination by the Sun or other sources, because it illuminate the ROI it self. For visibility, the radar waves are not damped by clouds, rain, and snow the way visible light is.

[13]The Ground segment of a satellite system, such as the infrastructure found on Svalbard

4 Bistatic SAR

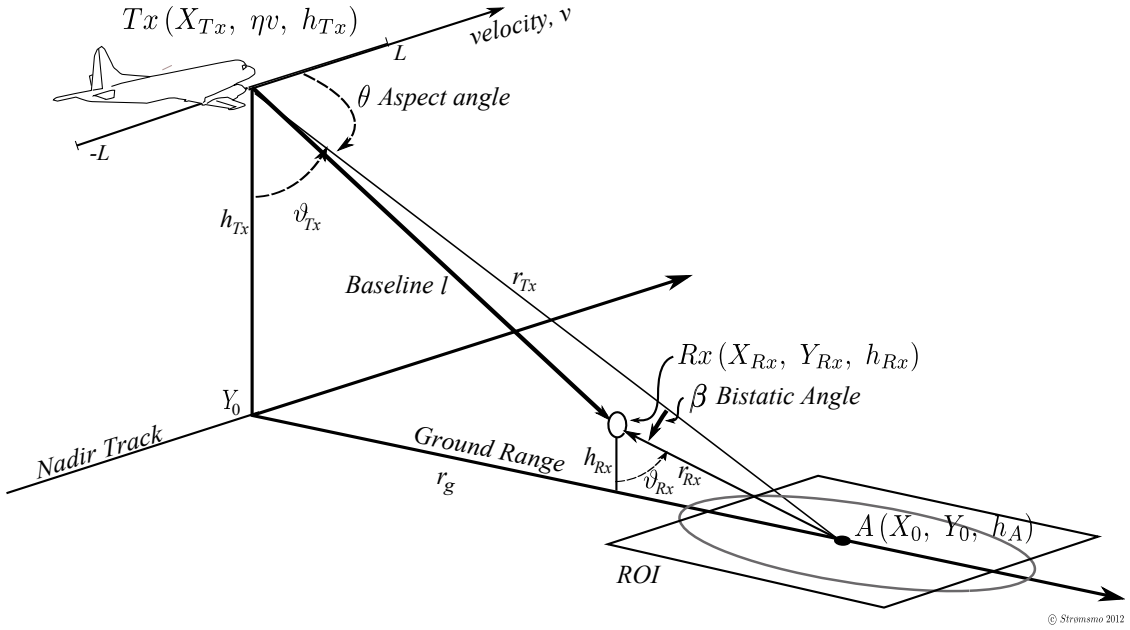

Figure 12: Bistatic SAR system with airborne transmitter and fixed receiver

4.1 Introduction

The difference between the monostatic and bistatic configuration is not as trivial as it might appear. A system is called bistatic when [1]

> *A radar using antennas for transmission and reception at sufficiently different locations that the angles or ranges to the target are significantly different.*

This is illustrated with the baseline l and the bistatic angle β in Figure 12. Transmitter and the receiver platforms might not share trajectories. In those cases the baseline is continuously changing throughout the imaging scenario.

In this chapter, the basics for a bistatic SAR system are presented, such as the geometry, signal properties, physical limitations. The geometry used in this thesis is shown in Figure 12, and it is limited to handle a fixed receiver, a transmitter flying in a direct line with an antenna pointing perpendicular to this flight path. With the geometry as base, the signal is elaborated with range and azimuth compression that focus the image. In preflight preparations, precautions to avoid distortion made by the topography is essential. Such limitations are presented in the end of this chapter. Also, limitations such as receiver antenna main lobe, and receiver bandwidth are defined.

The concept of hitchhiking receiver implies that the transmitter do not necessary know the receiver, and the performance of the monostatic system is not affected by this add-on device.

Although a bistatic SAR system leads to severe computation challenges, the parameters treated here are optimal [18]; X-band[14], fixed receiver, and zero squint[15] .

[14] 8–12 GHz, IEEE std [1]

[15] Squint angle is where the antenna is turned forward or backward compare to $\theta = \pi/2$

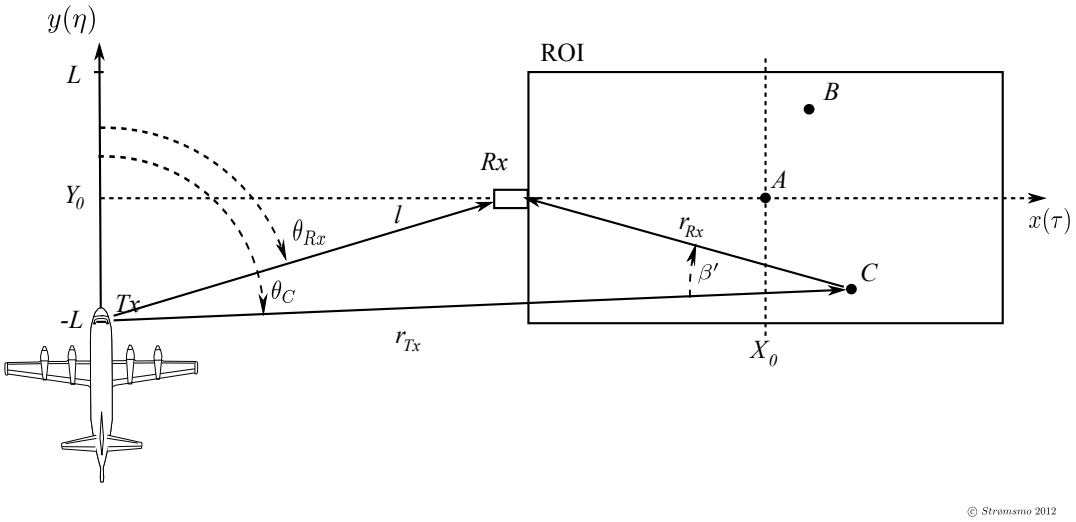

Figure 13: Geometry for bistatic configuration

4.2 Geometry

The bistatic configuration differs from the monostatic configuration by its geometry. Even though, a "bistatic configuration" classification still does not define the system good enough. The relation between scene, transmitter-platform, receiver-platform, transmitter antenna, and receiver antenna have to be explained.

In this thesis, the configuration is optimized to minimize computational load and algorithm-design. This is achieved by having

- a squint-angle approximately equal zero for the transmitter,
- transmitter platform that flies in a straight line with constant velocity v,
- a stationary receiver mounted on a hill above the scene,
- no moving objects to be corrected,
- and a large off-nadir angle which can simplify $r_s \approx r_g$

as illustrated in Figure 12.

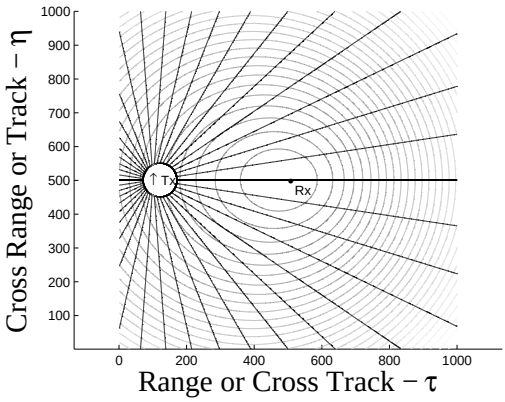

Figure 14: ISO Range and Doppler for bistatic configuration with fixed receiver

To relate this data to the already mentioned NED system in 3.2, the parameters becomes

- Point A at Scene center; $A\,(X_c,\ Y_c,\ 0)$ (same),
- Transmitter platform; $P_{Tx}(\eta)\,(0,\ \eta v,\ h_{Tx})$ (same),
- Receiver platform; $P_{Rx}\,(X_{Rx},\ Y_{Rx},\ Z_{Rx})$ (fixed),
- **bistatic baseline** $l(\eta) = P_{Tx}(\eta) - P_{Rx}$ (hyperbola),
- **bistatic angle** $\beta(\eta) = \arccos \frac{(\mathbf{r}_{Tx}(\eta)\cdot\mathbf{r}_{Rx})}{||\mathbf{r}_{Tx}(\eta)||||\mathbf{r}_{Rx}||}$
- Slant-range; $\mathbf{r}_s(\eta) = \mathbf{r}_{Tx}(\eta) + \mathbf{r}_{Rx} - l(\eta)$ (hyperbola + constant - hyperbola) where;
  - $\mathbf{r}_{Tx}(\eta) = A - P_{Tx}(\eta)$
  - $\mathbf{r}_{Rx} = P_{Rx} - A$
- $r_g \approx r_s$.

η is the azimuth time, or slow-time parameter. It is basically the Pulse Repetition Interval (PRI) for the transmitter, which is similar for the bistatic case as the monostatic case shown in Section 3.2.

4.3 Two dimensional Signal $s(\tau, \eta)$

In contrast to the monostatic case, Figure 14 illustrate a dynamic situation of the range cells and Doppler lines that corresponds to the bistatic case. Areas where the range circles and Doppler lines are almost parallel, the radar has little, or no data to distinguish point scatterers. Although the bistatic configuration has some blind spots, the area to the right of the receiver has increased range resolution due to the greater off-nadir angle of the receiver than of the transmitter. The area between the transmitter and receiver has decreased range resolution, illustrated by the increased interval of the circles that represent range cell.

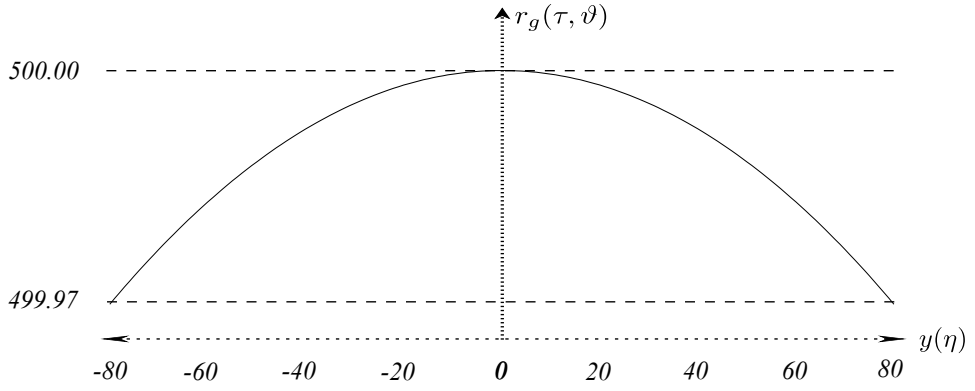

Figure 15: Bistatic ground range signature of point scatterer A

4.3.1 Range (τ)

The point scatterer range signature is the major difference between the bistatic and monostatic configuration. For the monostatic case, the pulse goes forth and back, while the pulse in the bistatic concept has to go the distance $r_{Tx}+r_{Rx}$, illustrated in Figure 13. And for the receiver, this echo is not accounted for until the direct pulse has gone the distance from the transmitter to the receiver, following l in the same figure. This means, for every row in the raw data — every PRI, the range signature is given by the propagation speed of the pulse traveling the distance $r_{Tx}+r_{Rx}-l$. The bistatic version of (22) becomes

$$\tau_n = \frac{r_{Tx_n}}{c} + \frac{r_{Rx_n}}{c} - \frac{l}{c}. \tag{28}$$

Both $r_{Tx}$and l are function of η, which gives a signal

$$s(\tau,\eta) = \int_x f_0(\tau) p\left(\tau - \frac{r_{Tx}(\eta)+r_{Rx}-l(\eta)}{c}\right) \tag{29}$$

where f_0 is considered as an ideal target function (See Appendix A.1 for definition).

A comparison of the monostatic ground range signature, given in Figure 7, and the bistatic signature in Figure 15, the hyperbola have opposite polarity. Also, the bistatic hyperbola spans from 499.97 meters to , which is only 3cm, while the monostatic hyperbola varies from 5500.56 to 5500.00 — 56cm.

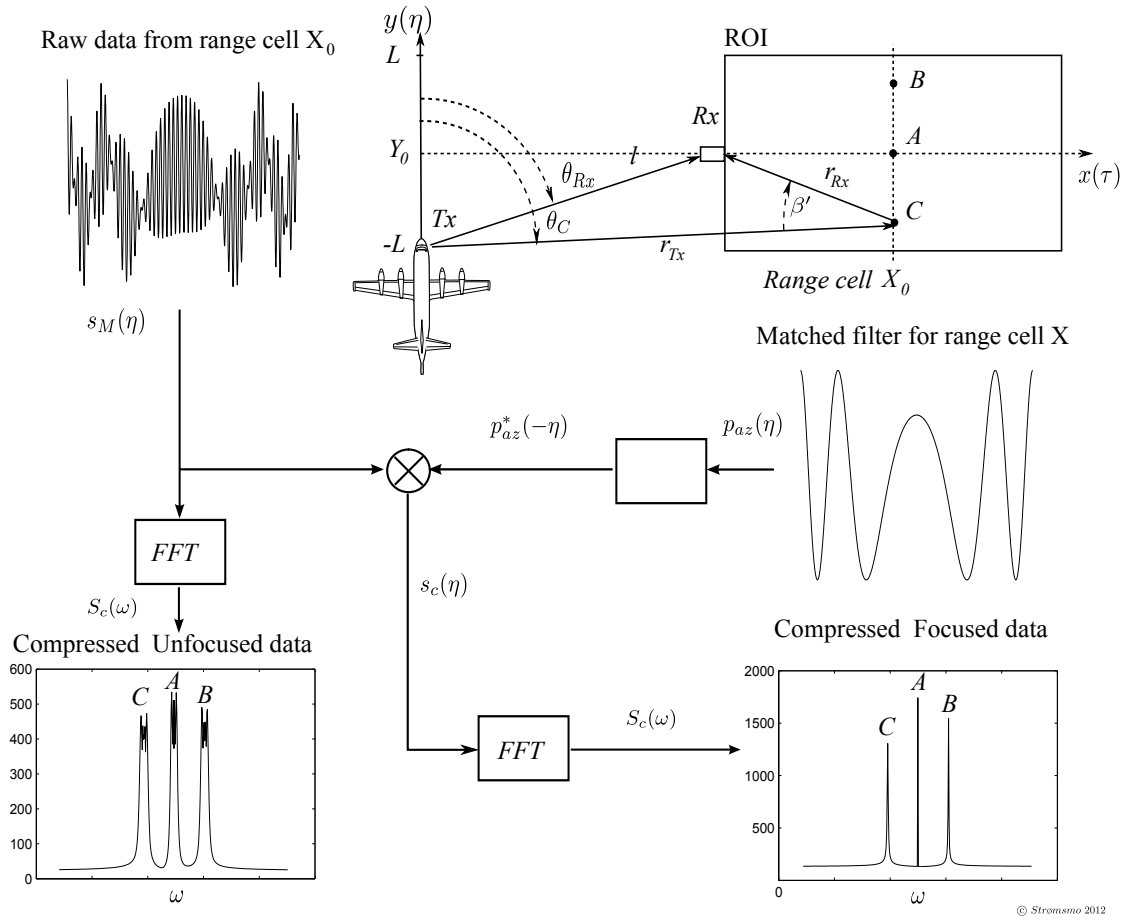

Figure 16: Azimuth compression of point scatterer A, B, and C

4.3.2 Cross Range (η)

Cross range for the bistatic system is derived in the same way as for the monostatic case. However, since it's the direct pulse that are used as filter reference for ranging, there is already some Doppler effect from the receiver mixed into the range compressed echoes. The Doppler dynamic that is left for cross range compression focusing is the difference in Doppler between the point scatterers echo and the direct pulse. The monostatic azimuth chirp function (26), in a bistatic hitchhiking case, becomes

$$\omega_{d_{C-bistatic}} = \omega_0 \frac{v}{c} \cos\theta_C - \omega_0 \frac{v}{c} \cos\theta_{Rx}, \tag{30}$$

where θ_{Rx} is the aspect angle to the receiver.

In Figure 16, the azimuth ranging axis is in wave domain ω. Tthe monostatic azimuth data were converted back to time domain, and azimuth axis is represented by azimuth time η, or PRI.

4.3.3 Raw data array

If the same scenario as shown in 3.3.3 were carried out with a bistatic SAR system, the signature of the three point scatterers will appear quite different. The receiver is placed in $Rx(5km,\ 0,\ 100m)$, illustrated in Figure 13 and 16.

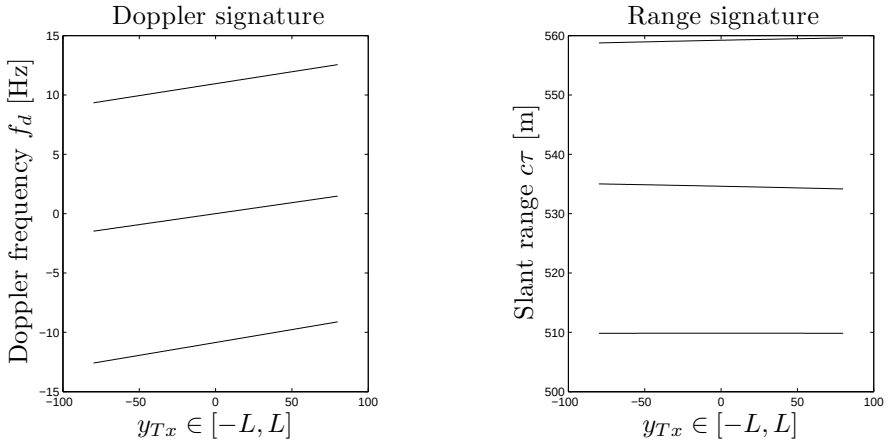

Figure 17: Doppler and Slant range signature for Point scatterer A, B, and C

Doppler frequency generate azimuth chirp which is an up chirp. In the monostatic case in Figure 9, the chirp were a down chirp. This is based on the geometrical conditions, where the receiver is placed closer to nadir track than the scene. This gives a $d\theta/dt$, from (11), that are greater for the receiver than the echoes from the scene, and when they are mixed in the range compression, the products are azimuth chirps, that are up chirps.

This matched filter process gives less dynamic chirp rate than the monostatic process. For point scatterer A, which has the Doppler frequency crossing zero Doppler, the chirp rate ω_c is approximately $\frac{3Hz}{5s} = 0.6 \rightarrow \omega_c = 1.2\pi$.

4.4 Distortion

Distortion that applies for a monostatic SAR system also applies for the bistatic. However, they will have deeper impact in some cases. Due to the great off nadir angle, shadows for the receiver antenna will be greater than for the transmitter antenna. And they might not share LOS. This means that even if objects are illuminated by the transmitter, the reflected signal might not reach the receiver. Or the opposite case, even if the receiver have good visibility of some object, they will not be detected unless they are illuminated by the transmitter.

Layover, where $\rho > \vartheta$ from Figure 10, will be reduced. This is due to the fact that the layover is given by the receiver's off nadir angle. If the receiver is placed at an altitude approximately zero, ρ as to be greater than $\pi/2$ for layover to act.

In a bistatic configuration, the geometrical distortion have a deeper impact on the degradation of the imaging process. Due to the lower height of the receiver, more shadows will occur. This leaves challenges to the planning of an imaging scenario, where to place the receiver relative to the scene and transmitter.

4.5 Limitation and usage

The fact that a bistatic system suffers from increased shadowing, the usage of a bistatic system needs more planning than with a monostatic system. It's important that the receiver has LOS to the scene, and the transmitter has LOS to the same area. This is achieved by placing the receiver in a high mast or on hill top. Placing the receiver in a hill side might put the receiver in the shadow of the transmitter, and then the system will not get the direct pools. The loss of this pulse will

make the system collapse as there is no synchronization between transmitter and receiver, and the range compression's matched filter will have no reference.

The receiver antennas main lobe must also be taken into account. The lobe will have a given sector were the antenna amplification is sufficient. The sector might be increased with the cost of reduced SNR. A special designed antenna could be the solution. An antenna with wide and flat main lobe. Also, several receiver antennas can be combined to create a wide receiver area for the bistatic system.

In the designing of the bistatic receiver, the ADC sampling rate has to be twice as the expected Doppler frequency, the Nyquist criteria mentioned in Section 2.

The great benefit, or potential, for a hitchhiking bistatic system is that the transmitter does not have to be dedicated. As the direct pulse is used in the range compression, the pulse can consist of anything from traditional LFM radar pulse to digital video broadcasting. The RF part of the system have to be designed for that frequency band though.

The bistatic system might also have a fixed transmitter and a moving receiver, or both moving. Both moving might be preferred in a conflict area, where the transmitter might be the AWACS [13], and the receiver in a Predator UAV [24][36]. This might prevent that other detects the imaging scenario, and safety for personnel and equipment can be increased.

For flooded areas, several receiver can be deployed around a ROI, keeping an optimal coverage and short data link from SAR system to the unit that examines and minimize the destruction.

5 Experiment

Figure 18: EKKO II trailer and the FFI Science team

Before a bistatic imaging scenario is tried out with a satellite as transmitter platform, a more affordable test environment can be used to optimize components and procedures. This experiment hitchhiked on a joint[16] experiment performed by the LUFO II project at FFI [15].

On the 14th of September 2011, a helicopter carried the PicoSAR and took several flybys past the Kjeller[17] area. While these flybys took pace, the PicoSAR illuminated the ROI with a scene center at latitude $\varphi_c = 59.97722$, and longitude $\lambda_c = 11.04662629$. HEL were placed at a hill North-East of scene center with latitude $\varphi_{Rx} = 59.97814$, and longitude $\lambda_{Rx} = 11.05589$. The image processed in this thesis were taken when the PicoSAR were at latitude $\varphi_{Tx} = 60.011599462$, longitude $\lambda_{Tx} = 11.11538$.

[16] Airborne Surveillance (LUFO II), Support to F-35 program, Operative Electronic Warfare Support (OPEK II), Technology for military vehicles.

[17] Skedsmo, Norway.

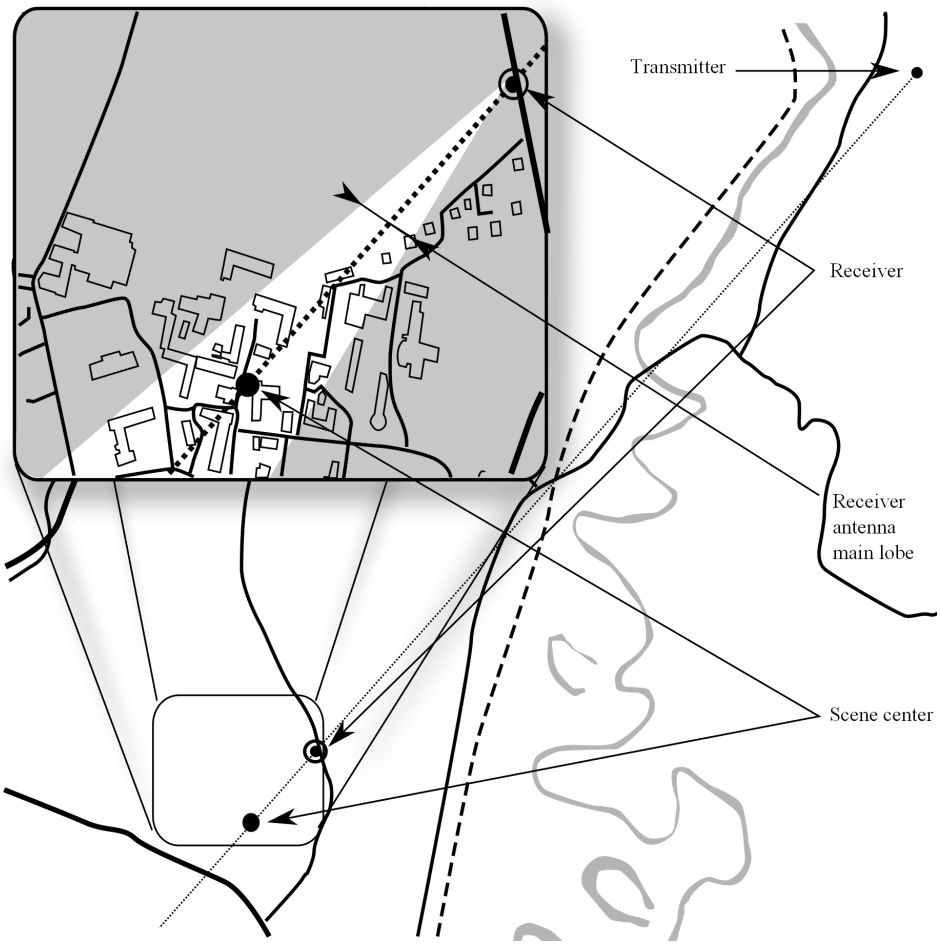

Figure 19: Practical Test Environment

5.1 Introduction

When PicoSAR got near $(\varphi_{Tx},\ \lambda_{Tx})$ it started to pump out LFM pulses at a Pulse Repetition Frequency (PRF) of 1kHz. The pulses reached the receiver as well as the scene. With a sample rate of 500MHz, HEL collected the direct pulse and the back scattered echos from the scene. Both channels were stored by two separate fast memories through the sequence. After a few seconds, PicoSAR were done pumping out pulses and HEL stopped recording. After recording, raw data were transferred to a disk and converted to ASCII-code. A 2.7GB file with raw data was the product so far.

The next step were to extract the optimal data from that data set. Desired info was extracted with Matlab and converted to an array with complex numbers and moved to base band[18]. Mirrored frequencies are filtered out and range compression is done by convolution of the echoes and the corresponding direct pulses.

Finally, an azimuth compression were performed, with no azimuth FM-rate correction in Result One, and with correction in Result Two.

[18]Base band is the signal without any carrier frequency component [5].

5.1.1 The Scene

Figure 20: Optical image of the Scene, downloaded from www.finn.no

The scene, shown in Figure 20 and sketched in Figure 19, consisted mostly of urban structures. This type of environments generate good signatures for testing, due to straight lines that may represent buildings, numerous of corner reflectors, predictable shadows, and metal structures with large radar cross section.

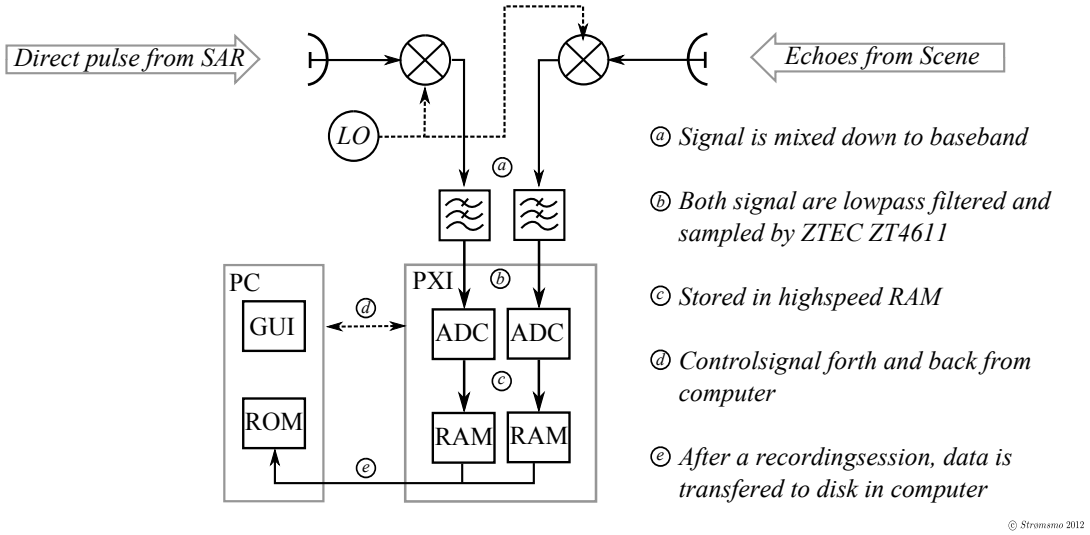

Figure 21: Sketch of HEL's components

5.1.2 HEL - Hardware

For the time being, HEL is mounted in the EKKO II trailer. This trailer contains antennas, rack, computer and power which is crucial for the system to work.

The system consists of two horn antennas, where one is pointed towards the expected position of the PicoSAR and the other points towards the scene, collecting direct pulse and echo respectively. They were turned 45° due to uncertainty of the PicoSAR's polarization. These horn antennas are connected by coax to Low Noise Amplifiers (LNA) and mixed to IF by two separate mixers with a shared LO. This base band signal is filtered by low pass filters and sampled by two separate Digital Storage Oscilloscope (DSO) of the type ZT4611 from ZTEC, Attachment Two gives the manufacturer's presentation. The DSO were configured to record for a given time for each direct pulse on both channels. In this way, two array is formed. One with the raw data from the scene, consisting range, τ, and azimuth, η, data. And one that holds the reference pulse for each η row. The data that is stored in the Random Access Memory (RAM) of the two DSO units are transferred into the hard drive of a computer. This computer also has a LabVIEW Graphical User Interface (GUI) that makes it possible to the operator to control the system.

5.1.3 PicoSAR

The SAR used in this experiment was a PicoSAR Beta version by Selex Galileo, see Attachment Three for description. It is a 10kg X-band SAR with image resolution of 1 meter in range and cross range. It also has a spotlight mode where the resolution get increased to 30cm in both range and cross range. The SAR were mounted in a Helicopter and operated by two FFI scientists.

The PicoSAR took several monostatic images, and the image that correlated best with the bistatic image in Figure 24 were picked out to be the reference image in Figure 23. All images taken by the PicoSAR had a header file with the time the image were taken, GPS coordinate for the SAR platform, velocity, carrier frequency, and PRF. This data is necessary to azimuth compression chirp calculation.

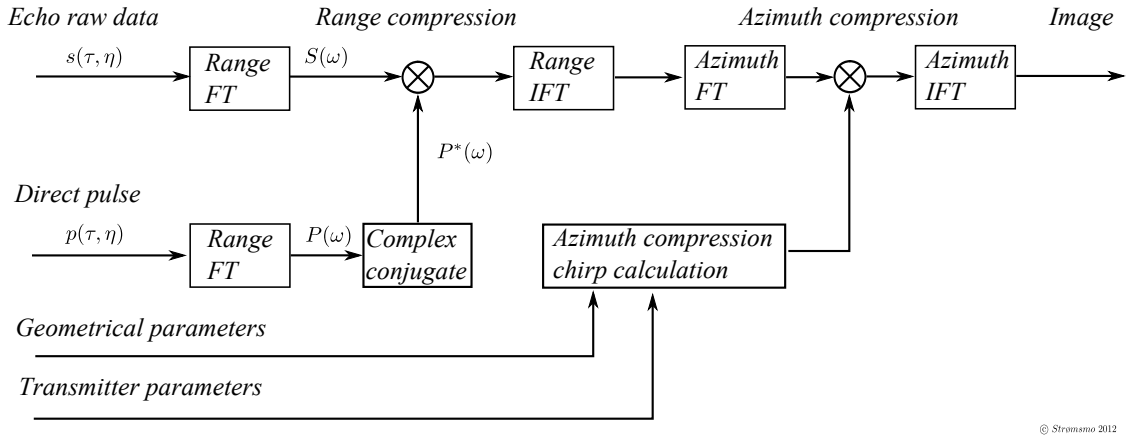

Figure 22: HEL software functional block diagram

5.2 Hardware setup and limitations

HEL were placed at the *receiver position* in Figure 19. PicoSAR was at *transmitter position* in the up right corner of the same figure, and the scene center was at *scene center*.

Because there is few hills and masts around the area available, the receiver had very high off nadir angle ϑ to the scene. This resulted in shadowing from the tall buildings in the front, shown in the top image of Figure 18.

The receiver antenna of HEL that pointed towards the scene center had a main lobe of approximately 16° for frequencies around 10GHz[19]. The sector of antenna is illustrated in Figure 19.

5.3 Software

In this experiment, the algorithm to focus the raw data set will be a simplified approximation of the *NLCS-algorithm for the stationary receiver case* described in [18]. The DSP was written in Matlab, and all processing is done within this program.

5.3.1 Echo raw data

The raw data of the echoes were collected by the receiver antenna pointing towards the scene, illustrated in Figure 21. The data were recorded in a string of ACII codes that represented the sampled value given by the ADC shown in the same figure.

5.3.2 Direct pulse

For the direct pulse, the second antenna were pointing towards the expected position of the transmitter as the scene were illuminated by its pulses. In the same way as the back scattered data, the direct pulse were also stored in ASCII codes.

[19] From Technical Manual on Horn Antenna DRG - 4010/A. Antenna Research Associates, Inc. Approved December 1993

5.3.3 Transmitter parameters

The transmitter parameters such as velocity, PRF, and carrier frequency f_0 were extracted from PicoSAR image header file, of the reference image in Figure 23.

5.3.4 Geometrical parameters

After the bistatic imaging sequence were done, geometrical parameters were collected from the monostatic SAR systems imaging log for Tx data, and map application to find geographical positioning of receiver and scene. A function were written in Matlab to calculate slant range, baseline, and range to scene center at $y(\eta) = 0$ — Doppler centroid. The function is given in Appendix B.1.

5.3.5 Range Compression

The first task were to find the desired data of what was recorded, and a string of the direct pulse column of the data were plotted. This gave a readout of the quality of the pulses, and a pointer were set where pulses were optimal. It also gave a PRI which were used to make a function to read out automatically the desired data. There were 12667 samples in each PRI, and 2049 were used. 3960 pulses were range compressed, which had to be carried out in four steps due to Matlab maximum size limit of variables.

The direct pulse and the back scattered signal were stored in parallel. This made it easy to extract the pairs, the echo and the direct pulse. Range compression were performed by fast Fourier transform of both signals, remove the mirrored version of frequency and move the positive band to base band. The signals were inverse transformed, and the direct pulse were time reversed and complex conjugated. Finally, convolution between the back scattered signal, echoes, and the direct pulse were carried out.

The code is found in Appendix B.2.

5.3.6 Azimuth compression

For azimuth compression, the bistatic azimuth chirp had to be calculated for each range cell. The chirp were derived from the slant range function (20), that were convert to lambdas with (2), and finally to instant phase for each sample with (4). The phase function, which is a azimuth time η function, were used as the argument in (12). This azimuth chirp were used as matched filter for azimuth compression, See Appendix B.4 for code.

Azimuth resolution is given in wave-domain and not in azimuth time domain. The reason for this is that the elements in a range cell are divided by their Doppler frequency middle frequency, which is converted from a chirp to an approximately singular frequency that appear as a sinc in wave domain. This means that the data is not calibrated to actual ground range in azimuth.

5.4 Expected results

Desired result would be something near the image processed by the PicoSAR it self. The image generated by the PicoSAR, shown in Figure 23, corresponds very good with an optical image of the same scene. Buildings are easily picked out, even cars on parking lots. Fields appear as noise with shadows made by trees and bumps. Some artifacts works as corner reflectors for the

Figure 23: SAR image made by the PicoSAR

monostatic case and gives very high σ. Some are so high that the side lobes of the sinc in the azimuth compression procedure oscillate almost across the whole image.

The high off nadir angle of the monostatic image gives a very good base for comparison of the bistatic image.

5.5 Measured results

Images are color inverted due to readability on paper. For computer screen, black would be preferred as zero and white for intensity.

5.5.1 Result One, Figure 24

Azimuth compression were performed by a azimuth Fourier transform, as shown in Appendix B.3. The energy is represented by the frequency domain ω, as elaborated in 4.3.2 and 4.3.3, and not as η.

The collected data is also mainly collected from the 3dB lobe opening of the receiver antenna, illustrated in Figure 19.

The image appear as focused at the top, which it is based on the range compression of the reference pulse that have approximately the same Doppler component as the echoes from this area.

Further down in the image, point scatterer seems to be smeared out in azimuth — unfocused.

5.5.2 Result Two, Figure 25

Azimuth compression were performed by azimuth Fourier transform. Unlike the unfocused image, an nonlinear chirp were mixed into the received echoes before the transform. The chirp were found by predict the slant range change for every range cell in the image. In Figure 16, this effect is simulated, and Figure 25 verify the effect.

The image is still represented in ω domain in azimuth.

Figure 24: Result One: HEL-image without Chirp Scaling

Figure 25: Result Two: HEL-image with Chirp Scaling

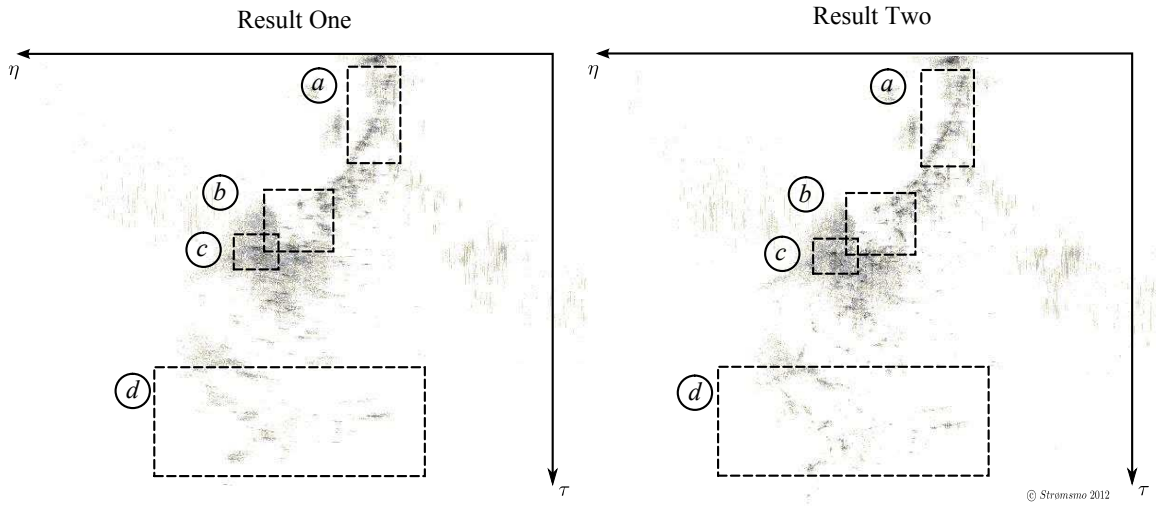

Figure 26: Comparison of Result One and Result Two

5.5.3 Image Analysis

In Figure 26, both the unfocused and the focused image are presented, left and right respectively. In the image analysis, four areas has been picked out;

a This area were close to the receiver, and the difference of the two images are not that significant. This is in accordance to the theory of azimuth compression, where the direct pulse with approximately the same azimuth chirp as point scatters in this area. Using the direct pulse in range compression removes also the azimuth chirp, and no focus handling is necessary.

b Here it is a shadow. The shadow has a distinct signature which is easy to find in the reference image too, shown in Figure 23. Both images have more or less same size and shape of the shadow. That would reflect that smeared returns are not smeared much .

c One point has good reflection in the bistatic concept, and the amount of improvement by focus the image can easily be seen her.

d Further out it the image, the need of focusing increase. Areas that may appear as noise in the unfocused image, can be addressed to objects when the azimuth compression is performed with a matched filter.

5.6 Conclusion

For starters, the impressive, and unexpected, result in Result One, Figure 24, is based on simplified compression of data. No parameters from the transmitter platform, such as carrier frequency, velocity, position, PRF, etc, are implemented in the algorithm. In spite of this, the image can represent the Region Of Interest (ROI). This is with a resolution that decreases further out in the image , i.e. with range. The reason for this is that the azimuth chirp is removed in the range compression sequence due to the Doppler shift in the direct pulse. Simulation in Figure 17 verifies this effect.

The improvement of image sharpness can easily be seen in Figure 26. The DSP demand high level of inputs, but the processing load is not too strenuous. The improvement is necessary to find the bistatic system useful.

In this experiment, the receiver antennas for HEL were adjusted to 45° polarization based on the unknown polarization of the transmitter. The fact that HEL recorded also back scatters with chanced polarization, while the PicoSAR did not, will contribute on changes in HEL images compared to the expected result [8].

Measured result corresponds to simulated effects in Section 4.

6 Conclusion and Future Work

In this thesis, the theory of complex sine signals was presented in Section 2. In this section, the Doppler shift component was elaborated, and how it's possible to extract the frequency of a Doppler in a received signal. With the refined Doppler component and reference signal, spatial movement could be found.

In Section 3, the signal model built in Section 2 was described to fit the monostatic SAR imaging scenario. All physical parameters were identified, so ranging and cross ranging could be performed by simple computation. Theory for the monostatic configuration was adapted to fit a more complex bistatic geometry in Section 4. The section of bistatic SAR imaging also elaborates the difference in azimuth compression by simulate three point scatterers A, B, and C. The same scatterers were azimuth compressed in Section 3 to make the differences obvious.

The usage of monostatic SAR systems and bistatic systems are presented, with their benefits and limitations compared to optical imaging.

Finally, an experiment was performed at Kjeller, Skedsmo. This experiment produced raw data that could be processed by the techniques developed and described in Section 4. Effects that were pointed out in bistatic azimuth compression were confirmed by the experiment, and focusing algorithm did improve image quality as simulation implied.

The theory given in Section 3 and 4 should give the reader enough understanding to work through Section 5.

The work done in this thesis shows that a bistatic SAR system with a stationary receiver, such as HEL, is feasible. The investigation around bistatic geometry and algorithm design shows that image range compression with the direct pulse gives benefits. However, focused azimuth compression can not be done without the knowledge of transmitter position, velocity, and flight direction.

Crucial knowledge for bistatic imaging is presented in this thesis. Also the differences between monostatic SAR and bistatic imaging that is necessary to develop bistatic imaging algorithms, or adapt known algorithms to fit a bistatic concept.

6.1 Conclusion of the experiment

HEL produced image in range, based on time, and cross range, based on frequency. A unfocused image that needed no filter design, and a focused that needed knowledge of the transmitter platform position and scene center position for the filter design.

The direct pulse for range compression were sufficient to make sense of the echoes. A focusing algorithm improved dynamics and details in the image.

6.2 Future work

First priority should be to make the output image of HEL correspond to ground range. In that case, components positions must be monitored accurate throughout the imaging process, so the aspect angle is known. Also the altitude of transmitter, receiver, and scene must be known. A Digital Elevation Map (DEM) used on the scene will improve the correction.

When HEL is able to generate images with correct geometry, the concept of add-on system or autonomous system will decide the hardware and software that should be used. Following concepts can be pulled through:

6.2.1 Slave receiver for space borne transmitter

This configuration would lead to a some processing implementation of satellite orbit data, such as the Two Line Element (TLE) data delivered from NORAD. This data contains the orbit parameters of a given satellite as well as its position in that orbit on a given time. By the use of the SGP4-model (Simplified General Perturbation No. 4)[20], this data can be converted to a Earth Center Earth Fixed (ECEF) frame, such as GPS coordinates. This would give a mission planning phase the sufficient data to perform an imaging scenario of a given ROI.

For an add on to a satellite system, transmitted pulses are known, with their carrier frequency and chirp rate. With this knowledge, azimuth compression can be done by a the known reference puls which are triggered by the direct puls, and traditional SAR algorithms might be used for image focusing.

6.2.2 HEL as a autonomous stand alone imaging system

This is where things get interesting. If the HEL could have the ability to image a scene almost without mission planning, it would be viable.

The first step would be to expand the receiving procedure of the direct pulse. By adding another two antennas and triangulating the direction to the source/transmitter would cover some of the input needed for the imaging algorithm. Reveling the pulse with no Doppler would give HEL an assumption about the carrier frequency ω_0 from 17. From this knowledge, the experienced Doppler shift can be extracted and compared to the triangulated position of the transmitter, which would reflect the transmitter velocity and flight direction. At the end of the day, all geometrical parameters are known, and SAR processing can be carried out of the received echos from the scene.

Iterative solution of transmitter velocity might also be solved by a auto focus algorithm.

[20] This model is optimized for Low Earth Orbit satellite, such as those used for remote sensing.

A Elaboration of Functions

A.1 Ideal target function

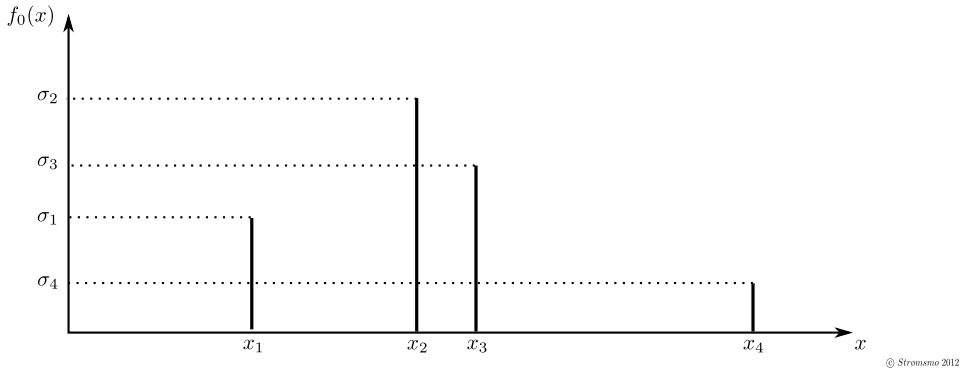

Figure 27: Ideal Target Function for four point scatterer

For an ideal echo of a target, there is no point spread function. The echo is considered as a Dirac delta function δ which is delayed by $x - x_n$ for the nth point scatterer. The reflectivity σ_n for the nth point scatterer is based on its material, shape and size. The function is given by Soumekh in [34] as

$$f_0(x) = \sum_n \sigma_n \delta(x - x_n)$$

A.2 Fourier transform of a function

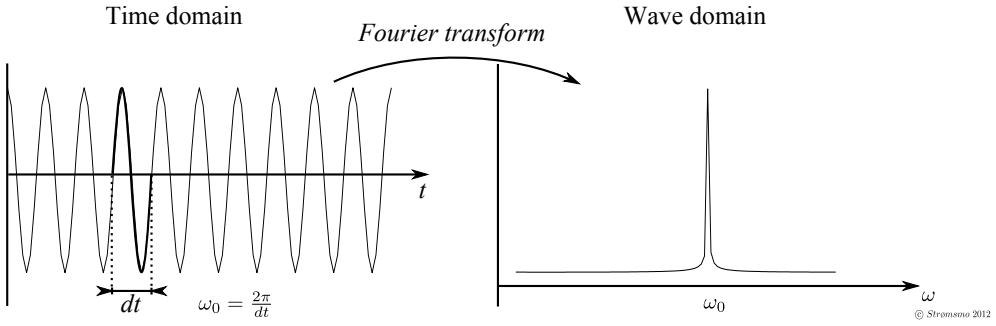

Figure 28: Fourier transform of a singular sine

From [26], Fourier transform is said to be

$$F(\omega) = \int_{-\infty}^{\infty} f(t) e^{-j\omega t}\, dt$$

B Matlab functions

B.1 Distance between two GEO points

The function is called geoVSgeo and finds the LOS distance between two given GPS coordinates.

```
function r = geoVSgeo(p1,p2)
a = 6378137;   % major axis (Equator) in meters
b = 6356752.3; % minor axis (Polar)   in meters
%%% Vector one %%%
p      = p1;
lati   = p(1)*pi/180;
longi  = p(2)*pi/180;
Re     = sqrt(((a^2*cos(lati))^2 + (b^2*sin(lati))^2)/...
                ((a*cos(lati))^2 + (b*sin(lati))^2));
R      = p(3) + Re;
% convert Vector one from geo to ECEF
X1     = R*cos(lati)*cos(longi);
Y1     = R*cos(lati)*sin(longi);
Z1     = R*sin(lati);
%%% Vector two %%%
p      = p2;
lati   = p(1)*pi/180;
longi  = p(2)*pi/180;
Re     = sqrt(((a^2*cos(lati))^2 + (b^2*sin(lati))^2)/...
                ((a*cos(lati))^2 + (b*sin(lati))^2));
R      = p(3) + Re;
% convert Vector two from geo to ECEF
X2     = R*cos(lati)*cos(longi);
Y2     = R*cos(lati)*sin(longi);
Z2     = R*sin(lati);
%%% Calculate the spartial distance %%%%
r      = sqrt((X1-X2)^2 + (Y1-Y2)^2 + (Z1-Z2)^2);
```

B.2 Raw data readout and range compression

```
clear;
close all;
%% Set system parameters
NumOfPulses              = 1000;
PulseWidth               = 3100;
SamplesPerPulse          = 12667;
NumberOfSamplesToRemove  = 8000;
DataSize                 = NumOfPulses*SamplesPerPulse;
SkipSize                 = (2136)*SamplesPerPulse;

%% Allocate memory and collect raw data 'Sample'
HRRP     = zeros(SamplesPerPulse-NumberOfSamplesToRemove+PulseWidth-1,NumOfPulses);
Filename='14092011_4.txt';

%% Find Reference Pulse end build matched-filter component 'b'
Sample   = dlmread(Filename,' ',[SkipSize3 0 SkipSize3+SamplesPerPulse 1]);
Ref      = Sample(1:PulseWidth,1);
Temp     = fft(Ref);
Temp(1:round(length(Temp)/2))= 0;
Temp     = circshift(Temp,round(length(Temp)/4));
Ref      = ifft(Temp);
b        = conj(flipud(Ref));

%% Extract desired raw data 'Data' and generate HRRP-matrix
for n=1:NumOfPulses
        Sample   = dlmread(Filename,' ',[SkipSize 0 SkipSize+SamplesPerPulse 1]);
        Data     = Sample(1:SamplesPerPulse-NumberOfSamplesToRemove,2);
        Temp     = fft(Data);
        Temp(1:round(length(Temp)/2))=0;
        Temp     = circshift(Temp,round(length(Temp)/4));
        Data     = ifft(Temp);

        % Range compression
        HRRP(:,n)= conv(Data,b);
        SkipSize = SkipSize+SamplesPerPulse;
end
```

B.3 Azimuth compression with no chirp focus

```
clear;
load('Y:\OPEK␣II\DP4␣Teknologi␣for␣radar-EK\Satellitt\Data\HRRP_3960.mat');
A       = fft(HRRP')';
A       = [A(:,3960/2:end) A(:,1:(3960/2-1))];
A       = fliplr(A);
```

B.4 Azimuth compression with NLCS

```
clear;
AF    = 2;% This Autofokus parameter adjust for error
load('C:\Documents␣and␣Settings\gso\Desktop\HRRP_3960.mat');% RAW data
[m,n] = size(HRRP);

% Transmitter parameters
c     = 2.99792458e8;       % Speed of light
PRF   = 1e3;                % PicoSAR PRF
v     = 36.8151;            % m/s of PicoSAR platform
f0    = 9.6e9;              % PicoSAR frequency
sR    = 5e8;                % sampling ratio in Hz of HEL receiver
k     = 2*pi*f0/c;          % wavenumber for system in vaccum
b     = c/(sR);               % spartial resolution of sampling in range

% Geometrical parameters
Tx    = [60.011599462,  11.11538,   1000]; % Transmitter position (lati, longi, and alti)
Rx    = [59.97814,      11.05589,    100]; % Receiver position (lati, longi, and alti)
X0Y0  = [59.97722,      11.04662629,  20]; % Scene center (lati, longi and alti)

% Geometrical conversion from GEO to NED
y     = linspace(-((n/2)*(v/PRF)),((n/2)*(v/PRF)),n); % Scenario -L to L, dimensions
B_    = geoVSgeo(Tx,Rx);
rTx_  = geoVSgeo(Tx,X0Y0);
rRx   = geoVSgeo(Rx,X0Y0);
B     = sqrt(B_^2 + y.^2);
rTx   = sqrt(rTx_^2 + y.^2);
for u = 1:m
        l       = rTx_ + 2*b*(u-m/2-1)+ rRx;
        l       = sqrt(l^2 + y.^2);
        l       = l - B;
        phase   = l*k;
        phase   = phase - min(phase);
        phase   = max(phase) - phase;
        GAZ     = exp(-1i*phase*AF);
        HRRP(u,:) = HRRP(u,:).*conj(GAZ);
        HRRP(u,:) = fft(HRRP(u,:));
end
HRRP = [HRRP(:,n/2:end) HRRP(:,1:(n/2-1))];
```

C List of Acronyms

ADC	Analog to Digital Converter; A sampler that measure the instant value of a signal with a given samplerate. The result is a history of values that represent an analog signal
CSA	Chirp Scaling Algorithm; Predict a Doppler shift (chirp) for each range cell and compensate for this in each range cell in the raw data.
DAC	Digital to Analog Converter; Reads out a serie of discrete values and convert them to a continuously varying signal
DBS	Doppler Beam Sharpening; Procedure to use Doppler shift in the echo to increase azimuth resolution.
DSO	Digital Storage Oscilloscop; ADC with memory
DSP	Digital Signal Processing; Modern approach were signals are sampled into discrete values and processed in processor-time.
EUSAR	European Conference on Synthetic Aperture Radar; Every even year, this confrence is arranged to exchange and present science on the topic of imaging radars
FFI	Forsvarets Forsknings Institutt; Norwegian Defence Reseach Establishment; A department founded by the Norwegian government
GPS	Global Positioning System; American satellite based navigation system that, by triangulation, gives the geographical position of a GPS-receiver. Normally an up date frequency of one hertz.
GUI	Graphical User Interface; Operating Software for the operator to control and observe prosesses in the system
HEL	Hichhiking Echo Location; Bistatic SAR receiver that borrow signal from a known transmitter and process image without any synchronization to the transmitter except a direct puls.
IF	Intermediate Frequency; The product of the Local Oscillator frequency and RF, and used in the conversion from analog to digital state of the signal.
IMU	Inertial Measurement Unit; with a given Degree Of Freedom, it can detect movement by inertial measurement; accelerometer and gyros.
LFM	Linear Frequency Modulation; A Linear increasing or decreasing frequency is modulated on a carrier frequency.
LNA	Low Noise Amplifier; RF amplifier used at the beginning in receivers
LO	Local Oscillator; A sine oscillator that produces a known frequency that is used to convert signal from IF to RF and RF to IF by mixers
LOS	Line Of Sight; Direct path between two points, and nothing solid to intercept
LUFO	Luftmilitær Overvåkning, Military air space surveillance

NED North East Down reference frame. X-axis points to the North, Y-axis points to East, and the tumb, Z-axis, in this right handed reference frame points down towards Earth center.

NLCS Non Linear Chirp Scaling; An algorithm that takes into account the dynamic slant range variation, up to forth derivative, that effect Dopper components in echos

OPEK II Operativ EK støtte til Forsvaret II, Electronic Warfare support for the military.

PRF Pulse Repetition Frequency; Refers to the number of pulses that are sent by the transmitter each second

PRI Pulse Repetition Interval; The time between two pulses that are sent by the transmitter.

RAM Random Access Memory; Quick read and write memory. Loses all data with power cut

RAR Real Aperture Radar; A radar with a narrow beam for azimuth resolution.

RF Radio Frequency; The signal that is transmitted on the air by antennas.

ROI Region Of Interest; A limited geographical area that are processed or described

SAR Synthetic Aperture Radar; Imaging radar that uses Doppler shift to provide increased Azimuth resolution.

SLAR Side Looking Airborne Radar; A RAR that have a beam pointing perpendicular to the flightpath

SNR Signal to Noise Ratio; A ratio that reflects the amount of energy of the signal with respect to the noise floor

SRTM Shuttle Radar Topography Mission, a mission carried out in February 2000. Covering the Earth from 56 degree South to 60 degree North.

UAV Unmanned Aerial Vehicle; Aircraft, with any shape and size, that can perform tasks without a pilot. Unlike drone, it may change task while opertating. A pilot can operate the vehicle from ground.

D List of Symbols

β	bistatic angle
β'	bistatic angle in the xy-plane for Doppler component computation
η	Slow-time, or azimuth time. Also represent the transmitter PRI
f	Frequency, Hz $\left[s^{-1}\right]$
f_0	Carrier frequency
f_c	Chirp frequency
f_d	Doppler frequency
l	Bistatic baseline
λ	Longitude
λ_n	Longitude of point-target n.
λ_c	Longitude of scene center
λ_{Rx}	Longitude of receiver
λ_{Tx}	Longitude of transmitter
ω	Angular frequency $= 2\pi f = \frac{d\psi}{dt}$
ω_0	Angular frequency of carrier wave
ω_c	Angular frequency of chirp, Chirp rate
ω_d	Angular frequency of Doppler frequency
$p(\tau,\eta)$	Direct signal from transmitter to receiver
$p_{az}(\eta)$	Azimuth compression filter
φ	Latitude
φ_n	Latitude of point-target n
φ_c	Latitude of scene center
φ_{Rx}	Latitude of receiver
φ_{Tx}	Latitude of transmitter
ψ_d	Doppler shift phase
ψ_0	Carrier frequency phase
ψ_{Rx}	Received signal phase
r_{Rx}	Range from Scene to Receiver Rx
r_{Tx}	Range from Transmitter Tx to Scene

ρ	Angle between topography and the assumption of flat Earth.
$s(\tau, \eta)$	Signal received from scene
$s_M(\tau, \eta)$	Range compressed signal from scene
$s_c(\eta)$	Azimuth compressed vector for given range cell
$S_c(\omega)$	Fourier transformed $s_c(\eta)$
τ	Fast-time, or range time
θ	Aspect angle between transmitter platform velocity-vector and LOS to object

References

[1] IEEE Aerospace and Electonic Systems Society. IEEE Standard Radar Definitions. *IEEE Std 686-2008*, 2008.

[2] IEEE Aerospace and Electronic Systems. Pioneer Award 1985, Carl A Wiley. *TRANSACTIONS ON AEROSPACE AND ELECTRONIC SYSTEMS*, AES-21 No.3:438–439, 1985.

[3] H. Assilzadeh and Y. Gao. Oil Spill Emergency Response Mapping for Coastal Area Using SAR imagery and GIS. *IEEE*, pages 1–6, 2008.

[4] Ulrich Balss, Andreas Niedermeier, and Helko Breit. TanDEM-X Bistatic SAR Processing. *EUSAR 2010*, 8th:1–3, 2010.

[5] David K. Barton and Sergey A. Leonov. *Radar Technology Encyclopedia*. Artech House, Inc, 1998.

[6] Florian Behner and Simon Reuter. HITCHHIKER, Hybrid Bistatic High Resolution SAR Experiment using a Stationary Receiver and TerraSAR-X Transmitter. *IEEE*, pages 1030–1033, 2010.

[7] Antoni Broquetas, Paco Lopez-Dekker, Jordi J. Mallorqui, Albert Aguasca, Mario Fortes, Juan Carlos Merlano, and Sergi Duque. SABRINA-X: Bistatic SAR receiver for TerraSAR-X. *EUSAR*, 8th:1–3, 2010.

[8] James B. Campbell. *Introduction to Remote Sensing*. The Guilford Press, 2006.

[9] Sergi Duque, PacoLópez-Dekker, and Jordi J. Mallorqui. Single-Pass Bistatic SAR Interferometry Using Fixed-Receiver Configuration: Theory and Experimental Validation. *IEEE*, pages 2740 – 2749, 2010.

[10] Florence M. Fetterer, Denise Gineris, and Ronald Kwok. Sea ice type maps from Alaska Synthetic Aperture Radar Facility imagery: An assessment. *Journal of Geophysical Research*, 99:443–458, 1994.

[11] Thomas Fritz, Helko Breit, N. Adam, M. Eineder, and M. Lachaise. Interferometric SAR Processing: From TerraSAR-X to TanDEM-X. *EUSAR*, 7th:1–4, 2008.

[12] Oleg V. Goryachkin and Rashid R. Yangazov. Some Parameters of Bistatic SAR based on TV-Signals. *EUSAR 2010*, 8th:1–3, 2010.

[13] Eric Hughes and Thomas Wheeler. Evolving the Airborne Warning and Control System (AWACS). *Computer Software and Applications Conference*, pages 364–367, 1998.

[14] Atle O Knapskog. Moving Targets and Multipath in SAR Images of Harbour Scenes. *EUSAR 2012*, pages 547–550, 2012.

[15] Atle Onar Knapskog and Nina Ødegaard. Målekampanjer med PicoSAR i Oslo havn og Kjellerområdet høsten 2011. *FFI-rapport 2011/01924*, pages 1–33, 2011.

[16] V. Krishnan, C. E. Yarman, and B. Yazici. SAR Imaging Exploiting Multi-path. *IEEE*, pages 1423–1427, 2010.

[17] F. Kugler and I. Hajnsek. Forest characterisation by means of TerraSAR-X and TanDEM-X (polarimetric and) interferometric data. *Geoscience and Remote Sensing Symposium (IGARSS)*, pages 2578–2581, 2011.

[18] Neo Yew Lam. *Processing Algorithms for Bistatic Synthetic Aperture Radar Data*. VDM Verlag Dr. Müller GmbH & Co. KG, 2010.

[19] Robert Linnehan, Ross Deming, and John Schindler. Multipath Analysis of Dismount Radar Responses. *IEEE*, pages 474–479, 2011.

[20] Paco Lopez-Dekker, Sergi Duque, Juan Carlos Merlano, Juan Rodriguez-Silva, and Jordi J. Mallorqui. Fixed-Receiver Bistatic SAR Along-Track Interferometry: First Result. *EUSAR 2010*, 8th:1–4, 2010.

[21] Allan W Love. In the Memory of Carl A. Wiley. *Antennas and Propagation Society Newsletter*, pages 17–18, 1985.

[22] Xin Lu, Jieqoing Wang, Zhenghuan Wand, and Hong Sun. Flooded Area Detection using Multi-temporal TerraSAR-X data. *IEEE*, pages 155–159, 2009.

[23] Søren Nørvang Madsen. Estimating The Doppler Centroid of SAR Data. *Transactions on Aerospace and Electronic Systems*, 25:134–140, 1989.

[24] Matt J. Martin and Charles W. Sasser. *PREDATOR The remote-control air war over Iraq and Afghanistan: A Pilot's Story*. Zenith Press, 2010.

[25] Antonio Moccia and Alfredo Renga. Potentialities and limitation of hybrid space-airborne bistatic SAR. *EUSAR 2010*, 8th:1–4, 2010.

[26] Athanasios Papoulis. *Signal Analysis*. McGraw-Hill, Inc, 1977.

[27] Grzegorz Pietrzyk, Pitor Samczynski, Adam Gorzelanczyk, and Krzysztof Kulpa. Real-time Implementation of Doppler Beam Sharpening Technique with Simple Motion Estimation. *European Radar Conference*, pages 185–188, 2004.

[28] Cristian Rossi, Michael Eineder, Thomas Fritz, and Helko Breit. TanDEM-X Mission: Raw DEM Generation. *EUSAR*, 8th:1–4, 2010.

[29] Russell Rykhus and Zhong Lu. Hurricane Katarina Flooding and Oil Slicks Mapped with satellite Imagery. *Science and the Storms: the USGS Response to the Hurricanes of 2005*, pages 49–52, 2005.

[30] Jesus Sanz-Marcos, Jordi J. Mallorqui, and Albert Aguasca. First ENVISAT and ERS-2 Parasitic Bistatic Fixed Receiver SAR image processed with the Subaperture Range-Doppler Algorithm. *IEEE*, pages 1840 – 1843, 2006.

[31] Marcel J. Sidi. *Spacecraft Dynamics & Control A practical engeneering approach*. Cambrigde University Press, 1997.

[32] Merrill I. Skolnik. *Introduction to Radar Systems, 2nd edition*. McGraw-Hill Book Co, 1980.

[33] Merrill I. Skolnik. *Radar Handbook, Third Edition*. McGraw-Hill Book Co, 2008.

[34] Mehrdad Soumekh. *Synthetic Aperture Radar Signal Processing*. John Wiley & Sons Inc, 1999.

[35] Jeff Sutton. The Role of Imaging Radar in the Development of the Canadian Arctic: Background and Applications. *Arctic*, 44:122–129, 1991.

[36] James A. Winnefeld and Frank Kendall. *Unmanned Systems Integrated Roadmap FY2011-2036*. Department of Defence, USA, 2011.

[37] Frank H. Wong and Tat Soon Yeo. New Applications of Nonlinear Chirp Scaling in SAR Data Processing. *IEEE*, 39:946 – 953, 2001.

[38] Hugh D. Young and Roger A. Freedman. *University Physics*. Pearson Educaton Inc, 2008.

Master thesis project 2012
for
Stud. Tech. Georg Gardsteig Strømsmo

Bistatic SAR-system with stationary receiver

En haikende radar utnytter senderen til en annen radar, den ”haiker” på den andre radarens signal. Den haikende radaren har minst to mottagerkanaler med hver sin mottagerantenne. En mottagerkanal er rettet mot senderen og tar opp dennes utsendte signal. Den andre mottagerkanalen rettes mot målet som radaren ønsker å detektere/avbilde/måle på etc. Praktiske systemer som demonstrerer dette prinsippet har vært presentert nylig.

En haikende radar kan gjøres relativt liten og billig. Dette åpner for mange nye anvendelsesområder, som systemer basert på et stort antall nettede haikende radarer, eller at man implementerer en sekundær haikende radarfunksjon i andre typer systemer som har mottagerfunksjonalitet. Liten størrelse og vekt og lavt strømforbruk åpner også for radarbruk på nye ”plattformer” som f eks små UAV-er eller kanskje solcelle/batteridrevne systemer.

Det er i hovedsak to teknologier som har åpnet for billige og kompakte løsninger:

- Analog-til-digital omformere med tilstrekkelig ytelse innen dynamikk og båndbreddde
- Dataprosessering med ytelse nok til å prosessere de AD-omformede dataene i sann tid

Begge disse teknologiene er i dag kommersielt tilgjengelige som subsystemer (f eks innstikks-kort til PC/kort med USB-tilkobling) til overkommelig pris. Det er også overkommelig kompleksitet forbundet med å anvende dem siden de kan programmeres vha kjente høynivåspråk som C++, LabView eller Matlab.

FFI har et 2-kanals datainnsamlingskort av typen ZT4611 fra ZTEC Instruments som vi ønsker å teste ut som haikende radar. Kortet er montert i en PXI ramme og er sammenkoblet en tilhørende analogdel som flytter de to mottagerkanalene koherent ned i frekvens slik at systemet kan opereres i frekvensområdet rundt 10GHz.

Oppgave

Oppgaven går ut på å analysere ytelsen til haikende radar generelt, samt FFIs eksperimentelle system spesielt. Oppgaven skal ta utgangspunkt i en rombasert belyser, og TerraSAR-X og Cosmo Skymed kan benyttes som referansesystemer. I første omgang er hovedmålet å demonstrere at den haikende radaren kan produsere et SAR-bilde av jordoverflaten, men oppgaven bør også se på andre radaranvendelser.

Det vil bli gjennomført et feltforsøk i løpet av arbeidsperioden med radaren PicoSAR som belyser. PicoSAR er en luftbåren SAR-radar som eies av FFI. Den kan programmeres til å operere med signalparametere som ligner de som de nevnte satellittsystemene benytter. Resultater fra eksperimentet skal benyttes for å underbygge analysene. Masterarbeidet skal resultere i en rapport som gir grunnlag for dybdeforståelse av muligheter og begrensninger ved haikende radar. Rapporten skal basere sine konklusjoner på resultater fra simuleringene og feltforsøket med PicoSAR.

Deloppgaver

1. Gi en teoretisk beskrivelse av prinsippet med haikende radar, inkludert praktiske begrensninger (radarprosessering, dekning for mottaker etc.) som kan forventes i et ekte system.

2. Gjennomfør simuleringer som gir grunnlag for å studere dynamikken i situasjonen "haikende radar". Et minimum er at man simulerer situasjonen med en luft-/rombasert sender og en bakkebasert stasjonær mottager som skal avbilde jordoverflaten, eller stasjonære overflatemål. En utfordring for haikende radar er at mottageren i mange situasjoner får en lav innfallsvinkel og dermed er utsatt for skjerming. Dette bør inkluderes i simuleringene, gjerne ved å inkludere digitale kart. Det er tilstrekkelig med direkte line-of-sight vurderinger, avanserte propagasjonsmodeller er ikke nødvendig. Hvis tiden tillater det kan simuleringene utvides til også å analysere andre radarsituasjoner/scenarier.

3. Minst ett eksperiment/feltforsøk vil gjennomføres i perioden. Kandidaten forventes å ta aktiv del i eksperimentet og analysere innsamlede data. I den forbindelse må et program for grunnleggende radarprosessering utvikles. Dette programmet skal ta de innsamlede dataene fra de to mottagerkanalene (direktesignalet og det reflekterte signalet) som input. Disse signalene er reelle og ligger i frekvensområdet 0-90MHz, så de må først kvadraturkonverteres til komplekse signaler med senterfrekvens 0Hz, og deretter SAR-prosesseres.

Simuleringer og programmering gjøres fortrinnsvis i MatLab.

Generelt:
Det innledende arbeid og litteraturstudium skal være en naturlig forberedelse og klargjøring av det videre arbeid i hovedoppgaven og skal inneholde:

- Generell analyse av oppgavens problemstillinger.
- Analyse av aktuelle kravspesifikasjoner, retningslinjer, praktiske erfaringer og litteratur.
- Definisjon i forhold til begrensinger og omfang av oppgaven.
- Klargjøring/beskrivelse av de arbeidsoppgaver som må gjennomføres for løsning av oppgaven med definisjoner av arbeidsoppgavenes innhold og omfang.
- En tidsplan for framdriften av prosjektet.

Innen 4 uker etter at oppgaveteksten er utlevert skal resultatene fra det innledende arbeid og litteraturstudium være ferdigstilt og levert i form av en forstudierapport. Forstudierapporten skal godkjennes av veileder før kandidaten har anledning til å fortsette på resten av hovedoppgaven.

Resultater fra det innledende arbeid inkluderes naturlig inn i innledningen og andre kapitler i masteroppgaven. Framdriftsrapporter og eventuelle avviksrapporter kan legges som vedlegg til hovedrapporten. Ved bedømmelsen av arbeidet legges det vekt på at gjennomføringen er godt dokumentert.

Besvarelsen redigeres som en forskningsrapport med et sammendrag både på norsk og engelsk, konklusjon, litteraturliste, referanser, innholdsfortegnelse etc. Påstander skal begrunnes ved bevis, referanser eller logisk argumentasjonsrekker.

Ved utarbeidelsen av teksten skal kandidaten legge vekt på å gjøre teksten oversiktlig, velskrevet og godt dokumentert.

Materiell som er utviklet i forbindelse med oppgaven, så som programvare/kildekoder eller fysisk utstyr, er å betrakte som en del av besvarelsen. Dokumentasjon for korrekt bruk av dette skal så langt som mulig også vedlegges besvarelsen.

Oppgaveteksten skal vedlegges besvarelsen.

Dersom oppgaven utføres i samarbeid med en ekstern aktør, skal kandidaten rette seg etter de retningslinjer som gjelder hos denne, samt etter eventuelle andre pålegg fra ledelsen i den aktuelle bedriften.

Kandidaten har ikke anledning til å foreta inngrep i den eksterne aktørs informasjonssystemer, produksjonsutstyr o.l. Dersom dette skulle være aktuelt i forbindelse med gjennomføring av oppgaven, skal spesiell tillatelse innhentes fra ledelsen.

Eventuelle reiseutgifter, kopierings- og telefon-/telefaksutgifter må bæres av studenten selv med mindre andre avtaler foreligger.

Hvis kandidaten, mens arbeidet med oppgaven pågår, støter på vanskeligheter som ikke var forutsatt ved oppgavens utforming, og som eventuelt vil kunne kreve endringer i eller utelatelse av enkelte spørsmål fra oppgaven, skal dette umiddelbart tas opp med Høgskolen i Narvik ved veileder.

Arbeidet skal resultere i en sluttrapport med vedlagt CD/DVD som er grunnlag for evaluering og karaktersetting. Rapporten med tilhørende materiale skal leveres i èn uinnbundet signert original som lett kan kopieres, samt tre innbundne kopier (evt. ekstern(e) samarbeidspartner(e)s materiell kommer i tillegg og skal overleveres av studenten selv), samt ett eksemplar av rapporten i pdf-format, fortrinnsvis på den vedlagte CD/DVD. Det skal benyttes standard forside som finnes på HINs nett. Det henvises forøvrig til skrivet *Generelle retningslinjer for hovedoppgaven*, samt emnebeskrivelsen for hovedoppgave.

Rapporten med tilhørende materiale skal innleveres (evt. poststemples) senest innleveringsdatoen til avdelingskontoret ved Avdeling for teknologi ved HiN.

Extradition date: 23.01.2012

Submission date: 09.07.2012

Supervisor: Associate professor Raymond Kristiansen
Tlf. 76 96 61 96
rayk@hin.no

Advisor: Øyvind Thingsrud (FFI)
Tlf. 63 80 72 85
oyvind.thingsrud @ffi.no

Advisor: Stein Kristoffersen (FFI)
Tlf. 63 80 72 48
stein.kristoffersen@ffi.no

Narvik University College
Department of Technology

Supervisor
(sign)

ZT4610
Digital Storage Oscilloscope

Key Specifications

Platform:
PCI, PXI, LXI, VXI

Channels:
2 or 4

Resolution:
8 bit

Bandwidth:
1 GHz

Max Sample Rate:
4 GS/s

Max Record Length:
512M Samples

Overview

- Embedded 64 bit signal processing for high-precision vertical, horizontal, and frequency-domain measurements.
- Four calculation channels for waveform math, digital filtering, FFT, and more
- Four non-volatile reference channels for storing and comparing waveforms
- Store and recall instrument settings files from on-board non-volatile memory
  Multiple acquisition modes including averaging, high-resolution, peak detect, and envelope
- Advanced measurement modes include limit and mask testing, histograms, and gated measurements

Industry leading acquisition rates

- Real-time sampling up to 4 GS/s
- Equivalent sampling up to 200 GS/s g

On-board memory with up to 512M sample record length

- Continuous memory mode for deep waveform capture
- Segmented memory mode for analysis of repetitive signals and statistical analysis

www.ztecinstruments.com

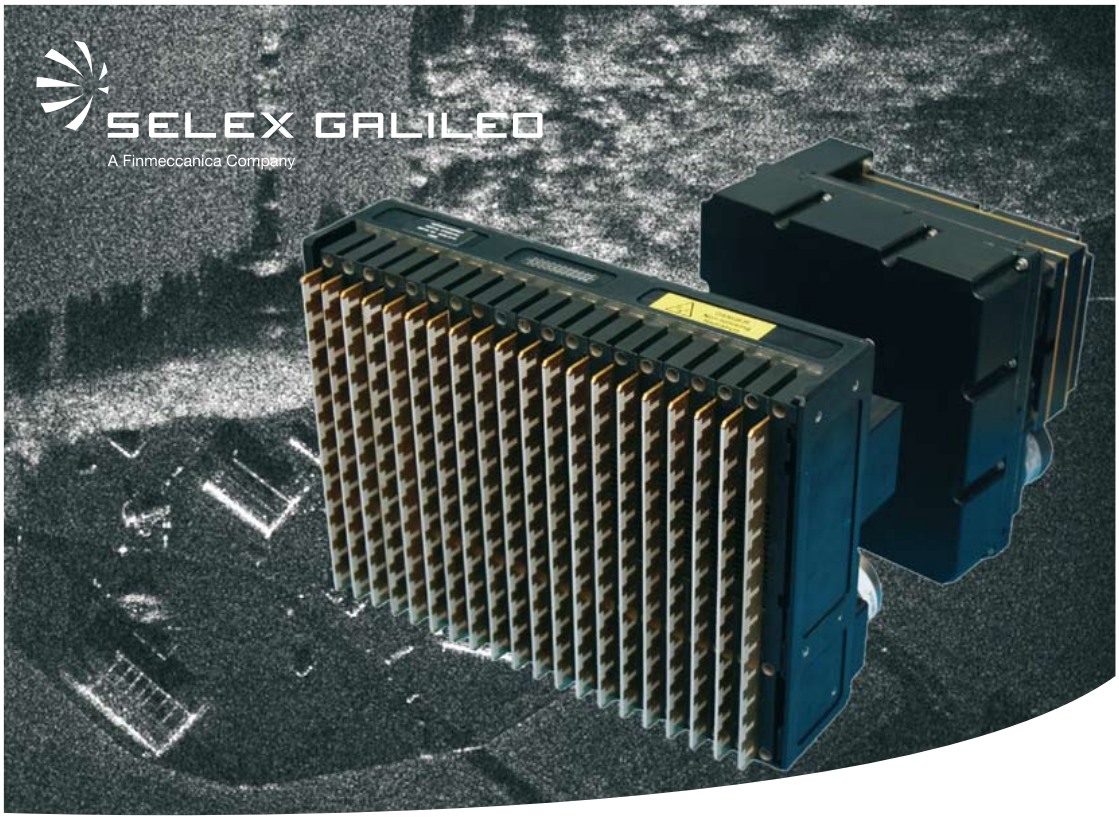

PICOSAR
COMPACT, LIGHTWEIGHT AIRBORNE GROUND SURVEILLANCE RADAR

The PicoSAR Active Electronically Scanned Array (AESA) radar provides an unrivalled all-weather capability for Unmanned Aerial Systems, fixed wing and helicopter platforms.

Building on over 50 years of experience in the airborne radar field, PicoSAR combines our knowledge with the latest technology to meet the evolving requirements of the 21st century.

KEY FEATURES

The key to PicoSAR is the use of AESA technology in a small, compact configuration. Using many low power, solid state Transmit/Receive Modules (TRM) within its array, the PicoSAR radar is more reliable than conventional radar systems.

For the most compact installations PicoSAR can be mounted directly onto the platform and the beam steered electronically, or it can be mounted on a gimbal for an even greater field-of-view.

PicoSAR consists of a single small Line Replaceable Unit (LRU). This LRU can be reconfigured if required to ease installation, by detaching the antenna unit from the processor unit.

In addition, due to the flexibility of AESA technology the radar antenna can be resized to address specific platform constraints or customer performance requirements.

PicoSAR delivers a high resolution Synthetic Aperture Radar (SAR) imaging and Ground Moving Target Indication (GMTI) capability that permits new and existing platforms to easily acquire a true, all-weather ground mapping and surveillance capability.

Its compact size, low weight and low power consumption permit installation in parallel with electro-optical/infrared sensors even on platforms with limited payloads.

KEY BENEFITS

- Excellent performance
  - High resolution ground mapping
  - Wide area coverage
  - High performance GMTI
- Low cost of ownership
- Reconfigurable radar system
- Lightweight
- Compact
- Very high reliability
- Easy to install
- Easy to use.